UCRL 15436
PREPRINT P.O. 2248301

UCRL--15436

DE82 011072

MASTER

Investigations on SYNROC Mineralogy

Progress Report to the Lawrence Livermore National Laboratory, As specified in Contract No. 2248301

A. E. Ringwood
Research School of Earth Sciences
Australian Natinal University

January 21, 1982

INVESTIGATIONS ON SYNROC MINERALOGY

Progress Report to Lawrence Livermore National Laboratory

January 21, 1982

As Specified in Contract No. 2248301

CONTENTS

Deddick Pty. Ltd.
3 Vancouver St.
Red Hill
Canberra A.C.T. 2603
AUSTRALIA

Manager and author of progress report: A. E. Ringwood

FACTORS INFLUENCING THE LEACHING PERFORMANCE OF HOLLANDITE

A.E. Ringwood, S.E. Kesson, V.M. Oversby and W. Hibberson

1. Introduction

An earlier report by A.N.U. (Ringwood et al., 1981a) studied the leaching of cesium from hollandite and SYNROC-C formulations. It was found that cesium was readily leached from samples hot-pressed under oxidizing conditions (near Ni-NiO) because cesium was not successfully immobilized in the hollandite lattice but had combined with molybdenum from the waste forming soluble cesium molybdate. This problem no longer occurred if hot-pressing was carried out under more reducing conditions (between Co-CoO and Fe-FeO) because molybdenum was reduced from the hexavalent state to Mo^{4+} and/or to a metal alloy; and Cs_2MoO_4 was destabilized.

However in subsequent experiments with hollandite and SYNROC formulations which contained no molybdenum, the leaching behaviour of cesium was still found to be very erratic, varying by as much as an order of magnitude, depending on hot-pressing redox conditions and sample preparation methods. This report evaluates the effects of such physical and chemical parameters on hollandite leaching performance and attempts to explain this in terms of hollandite crystal chemistry and reaction kinetics.

2. Starting materials and experimental methods

Table 1 lists the compositions of the various hollandite preparations used in this study. These were prepared by a range of techniques, and by three independant laboratories (see Table 1). Run products were examined by microprobe and x-ray techniques, and leaching tests carried out as described by Oversby and Ringwood (1981).

In most of the experimental studies described herein, microprobe investigations were largely directed at the one composition, "Cs-holl.mix I".

This composition (Table 1) corresponds to $BaAl_2Ti_6O_{16}$ (70 wt%) + TiO_2 (30 wt %) + an additional 2% Cs_2O. The excess of TiO_2 is present in order to maximise solid solution in the hollandite towards the hypothetical Ti-end-member "$Ba_oAl_oTi_8O_{16}$". Similar solid solutions occur in hollandite in SYNROC, because of the high TiO_2-activity of the SYNROC phase assemblage.

3. Effect of hot-pressing temperature on leach-rate

The composition "Cs-holl.mix I" was dried in air at 800°C. An additional 2% Ti retal was incorporated immediately prior to hot-pressing, in order to facilitate redox control (this topic is discussed further in Section 4 (b)). The samples were hot-pressed in Ni capsules at temperatures ranging from 1100 to 1350°C. The leach-rates obtained for these samples (Table 2) are illustrated in Fig.1. As in our earlier studies (Ringwood et al., 1981b) the leach-rates are observed to decrease markedly with time, falling by about an order of magnitude over seven days. The individual samples themselves yield leach-rate curves dispersed over about an order of magnitude (Fig.1). However it is apparent that the highest leach-rates occur in samples hot-pressed at temperatures of 1300°C or higher. The less-satisfactory leaching performance of these latter samples is tentatively attributed to incipient partial melting at near-solidus temperatures. Under such conditions some cesium may partition into an intergranular melt phase, from which it is then more readily leached.

4. Effects of hot-pressing redox conditions on leach-rates

(a) Redox conditions controlled by sample capsule

The composition "Cs-holl.mix I" (Table 1) was hot-pressed in Ni capsules at 5 kbar and temperatures from 1150°C to 1275°C. The same starting material was then hot-pressed in graphite dies at 4000 psi and

Table 1. Bulk compositions of hollandite starting materials

	S24 and S24-2A	S25 and S25-2A	S16	S03	H1-4	"Cs-holl. mix I"	"Cs-holl. mix II"
TiO_2	73.6	72.3	63.9		71.1	74.2	67.8
Al_2O_3	13.2	13.0	13.7		11.0	9.5	17.9
BaO	11.1	9.2	18.6		14.9	14.3	12.3
Cs_2O	2.3	5.6	3.8		3.0	2.0	2.0
Sum	100.	100.	100.		100.	100.	100.

Notes:

S24 corresponds to a composition with molar $(BaO + Cs_2O):(Al_2O_3):(TiO_2)$ = 1 : 1.6 : 11.4 and molar Cs_2O : BaO = 1:9. Prepared by L.L.L. from spray-dried nitrates (Memo; 2 February 1981).

S25 corresponds to a composition with the above molar ratios except Cs_2O: BaO = 1:3. Prepared by L.L.L. from spray-dried nitrates (Memo; 2 Feb. 1981).

S16 prepared by L.L.L. from spray-dried nitrates (Memo; 2 Feb. 1981). S16 is "stoichiometric" with molar$(BaO + Cs_2O) : (Al_2O_3) : TiO_2$ = 1:1:6.

S03 prepared by L.L.L. from spray-dried nitrates (Memo; 2 Feb. 1981) with molar $(BaO + Cs_2O) : (Al_2O_3) : TiO_2$ =

S24-2A and S25-2A are Sandia preparations of compositions S24 and S25 (letter; 27 Jan. 1981).

H1, H2, H3 and H4 correspond to four different preparations of the S16 hollandite composition to which an additional 20% of TiO_2 has been added. Their bulk composition is as shown. Preparations by R. Dosch, Sandia Labs., (Memo; 2 Dec. 1980).

"Cs-holl. mix I" corresponds to: 70% $BaAl_2Ti_6O_{16}$ + 30% TiO_2 + additional 2% Cs_2O (by weight).

"Cs-holl. mix II" corresponds to : 60% $BaAl_2Ti_6O_{16}$ + 30% TiO_2 + 10% Al_2O_3 + additional 2% Cs_2O.

Fig.1: Effect of hot-pressing temperature on leach-rate

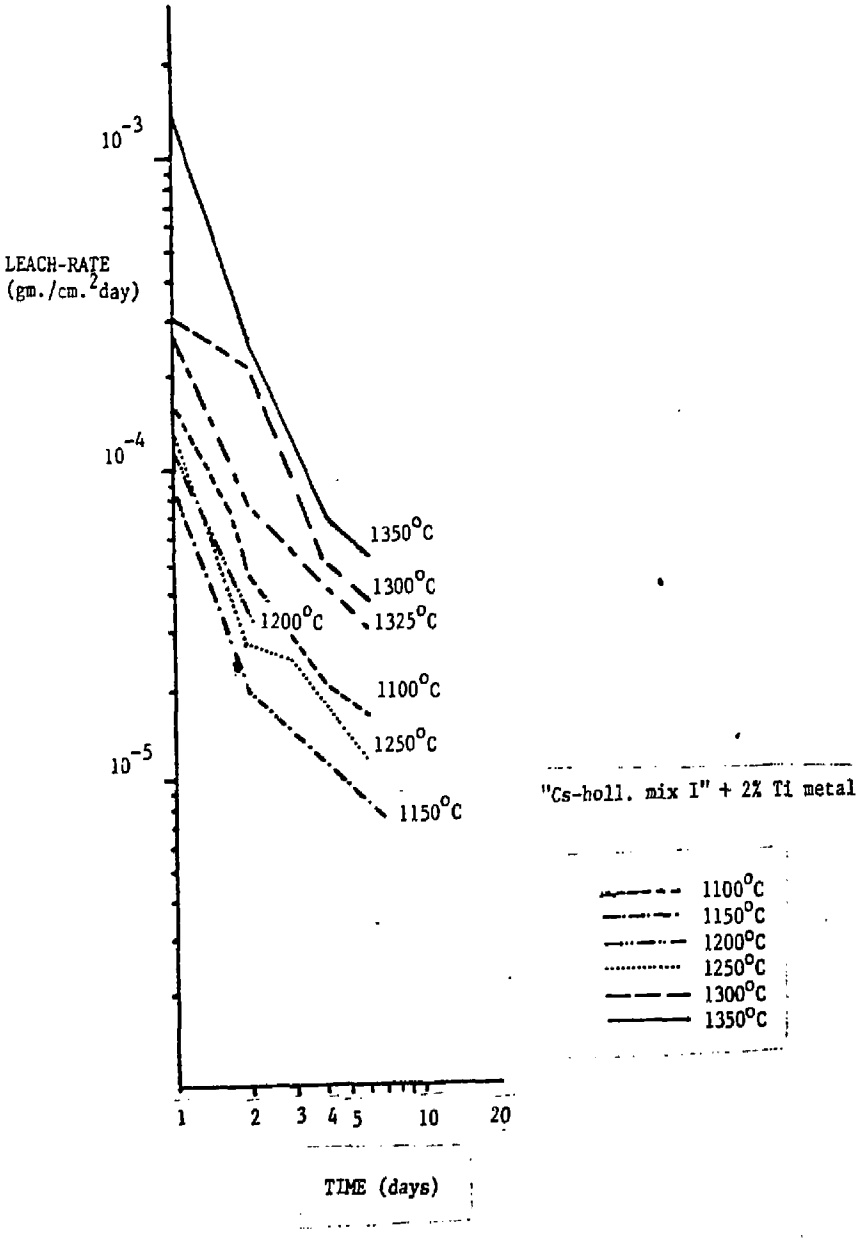

Table 2. Effect of hot-pressing temperature on cesium leach-rate

"Cs-holl. mix I" + 2% Ti metal hot-pressed in Ni capsules for 1 hour at temperatures shown

T°C	Day 1	Day 2	Day 3	Day 4	Day 6
1100	1.7×10^{-4}	4.6×10^{-5}		2.0×10^{-5}	1.6×10^{-5}
1150	8.4×10^{-5}	1.9×10^{-5}	2.2×10^{-5}	1.1×10^{-5}	7.4×10^{-6}
1200	1.2×10^{-4}	3.3×10^{-5}			
1250	1.4×10^{-4}	2.7×10^{-5}	2.4×10^{-5}	1.9×10^{-5}	1.1×10^{-5}
1300	3.1×10^{-4}	1.1×10^{-4}		5.0×10^{-5}	3.8×10^{-5}
1325	2.8×10^{-4}	7.6×10^{-5}		4.2×10^{-5}	3.2×10^{-5}
1350	1.4×10^{-3}	2.6×10^{-4}		6.9×10^{-5}	5.0×10^{-5}

Table 3. Cesium leach-rates for hollandite preparations hot-pressed in graphite or nickel

Experimental conditions: Graphite die, 4000 psi, 1 hour, temperatures as shown

Hollandite preparation	T°C	Day 1	Day 2	Day 3	Day 4	Day 6	Day 11
"Cs-holl. mix I"	1250	1.8×10^{-4}				1.3×10^{-5}	6.9×10^{-6}
"	1280	3.1×10^{-4}	3.4×10^{-5}		2.1×10^{-5}		
"Cs-holl. mix II"	1240	2.1×10^{-4}	7.4×10^{-5}		1.8×10^{-5}		
"	1290	4.3×10^{-4}	7.8×10^{-5}		2.4×10^{-5}		
"	1300	6.2×10^{-4}		1.0×10^{-4}		3.1×10^{-5}	

Experimental conditions: Nickel capsule, 5 kbar, 1 hour

"Cs-holl. mix I"	1200	1.4×10^{-3}	2.7×10^{-4}
"	"	1.9×10^{-3}	
"		5.4×10^{-3}	

Figure 2. Comparative leaching performance of hollandite preparations hot-pressed in graphite or nickel.

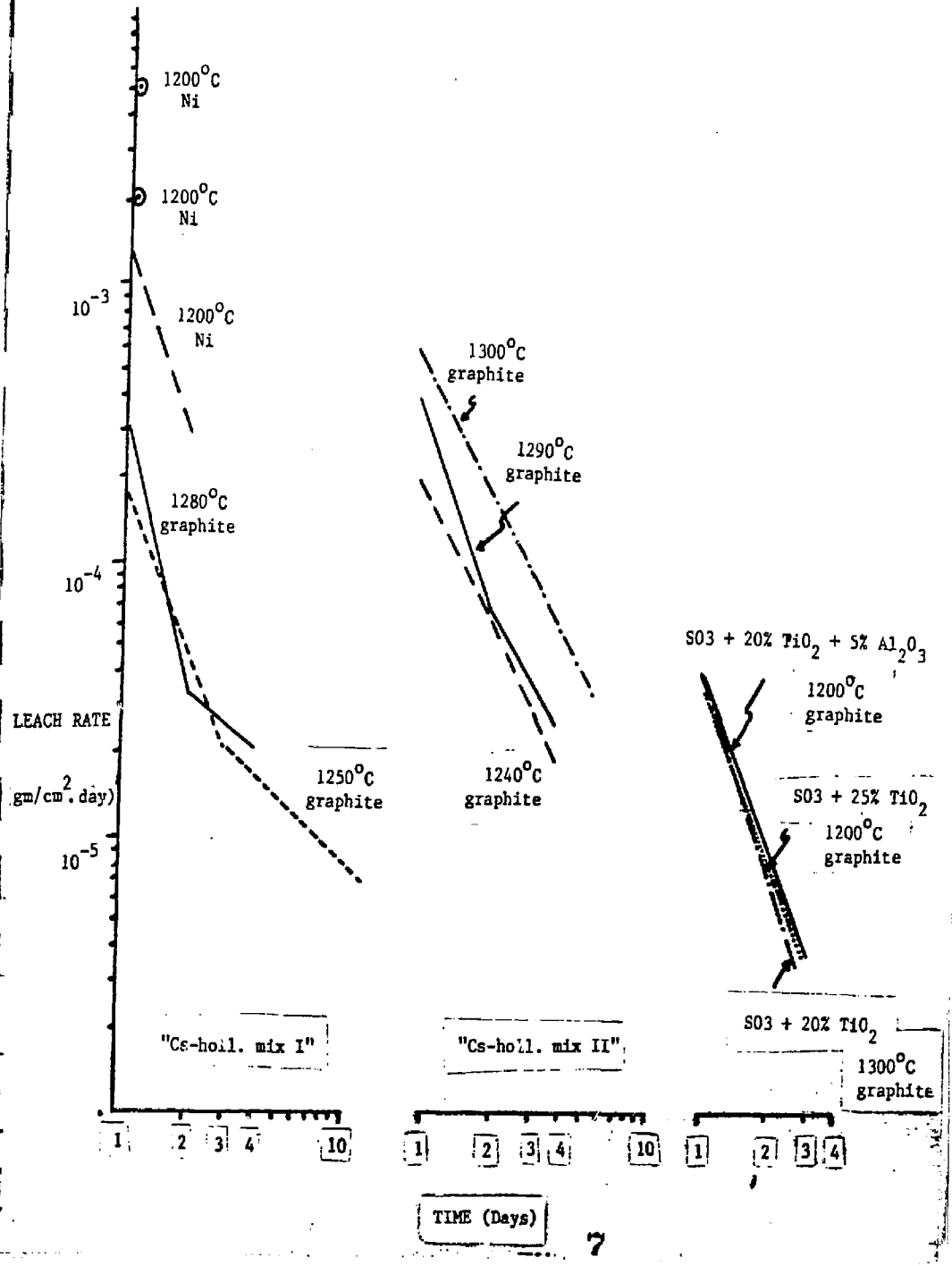

temperatures of 1250 and 1280°C. The products of these two series of experiments were leached at 95°C in H_2O, and subjected to microprobe analysis.

The leaching results are presented in Fig.2 and Table 3. The products of hot-pressing in Ni capsules display high initial leach rates, typical of hollandite hot-pressed under these conditions (compare with Fig.3). They lost a substantial proportion of their total complement of cesium on the first day, and for two of the three samples, no further leaching was carried out. In contrast, the leaching performance of the two samples hot-pressed in graphite is markedly improved, even the first day's leach rate being about an order of magnitude less than that for the samples hot-pressed in Ni.

Microprobe analyses of the runs (Tables 4 and 5) reveal that the product hollandites typically exhibit a range in composition, as indicated in the tables. In particular, cesium varies from below detection limits to an ideal maximum value of ~2%. (Mass-balance considerations suggest that cesium is not fully immobilized in hollandite; minor amounts of an unidentified Cs-rich phase may also be present in runs in both Ni and graphite.)

The most striking difference between the two sets of product hollandites is apparent in the unusually low Al_2O_3 contents and "non-stoichiometric" structural formulae of the samples hot-pressed in graphite. (Compare Tables 4 and 5.) Moreover, significant quantities of an aluminous phase (corundum or Al_2TiO_5) as well as rutile, are observed in the latter series.

In order to evaluate the structural formulae, it is important to bear in mind that there are three ideal end-members contributing to the hollandite solid solution series, namely:

$Ba\ Al\ Al\ Ti_6\ O_{16}$	cation sum = 9
$Cs\ Cs\ Al\ Al\ Ti_6\ O_{16}$	cation sum = 10
$Ti\ Ti\ Ti_6\ O_{16}$	cation sum = 8

Table 4. Hot-pressing of "Cs-holl. mix I" composition in Ni capsules.

T°C	1275°	1250°		1200°		1150°	
	Hollandite	Hollandites		Hollandites		Hollandites	
TiO_2	65.1	62.8	66.1	67.8	70.2	62.7	66.6
Al_2O_3	12.4	14.1	14.3	14.1	14.8	14.5	13.8
BaO	20.6	21.5	19.9	16.1	15.3	20.4	20.5
Cs_2O	2.1	1.6	0.2	1.8	.2	2.1	.2
Sum	100.2	100.0	100.5	99.8	100.3	100.2	100.9
coexisting phases	rutile rare corundum	rutile		rutile		rutile	
Structural formulae based on 16 oxygens							
Ti	6.103	5.897	6.001	6.107	6.132	5.877	6.043
Al	1.822	2.075	2.035	1.990	2.026	2.123	1.963
Ba	1.006	1.052	0.941	0.756	0.696	0.996	0.969
Cs	0.112	0.085	0.010	0.092	0.0	0.112	0.0
Sum	9.04	9.11	8.99	8.94	8.86	9.11	8.98
Ti+Al	7.92	7.96	8.03	8.09	8.15	7.99	8.00

Experimental conditions: Ni capsules, 5 kbar, 1 hour, temperature as shown.

Table 5. Hot-pressing of "Cs-holl. mix I" composition in graphite dies

T°C	1280°		1250°	
	Hollandites		Hollandites	
TiO_2	66.9	69.1	66.0	67.4
Al_2O_3	8.8	3.8	10.5	10.1
BaO	22.1	24.1	21.4	21.7
Cs_2O	1.7	2.9	2.2	0.8
Sum	99.5	99.9	100.1	100.0
coexisting phases	rutile corundum		rutile Al_2TiO_5	
Structural formulae based on 16 oxygens				
Ti	6.429	6.888	6.269	6.341
Al	1.325	0.594	1.563	1.489
Ba	1.107	1.252	1.059	1.064
Cs	0.093	0.164	0.119	0.043
Sum	8.95	8.90	9.009	8.936
Ti + Al	7.74	7.47	7.83	7.83

Experimental conditions: graphite die, 4000 psi, 1 hour , temperature as shown.

If redox conditions are sufficiently reducing to permit the partial reduction of Ti^{4+} to Ti^{3+}, then a further solid solution mechanism is permitted, namely $Ti^{3+} \rightleftharpoons Al^{3+}$. It should be evident that an acceptable hollandite structural formula need not possess an integral cation sum on the basis of 16 oxygens, because of the flexibility for filling the large cation sites. However the sum of Ti + Al (all sites) should be very close to the ideal value of 8.

Hollandites produced by hot-pressing in Ni (Table 4) in most cases exhibit a modest excess of TiO_2 i.e. structural Ti > 6 and cation sum < 9.0. In all cases, the sum (Ti + Al) is close to a value of 8.0, and the two Al-sites are fully occupied. On the other hand, hollandites produced by hot-pressing in graphite (Table 5) have insufficient Al to fully occupy the Al-site, a substantial excess of Ti is present, and the sum of (Ti + Al) is less than the ideal value of 8. All of these characteristics are consistent with reducing conditions permitting stabilization of significant amounts of Ti^{3+}, with its subsequent entry into the Al sites. (The low sum of Ti + Al in an artifact arising from the analytical data, because the microprobe cannot discriminate between Ti^{3+} and Ti^{4+} and automatically computes all titanium as TiO_2.) The "surplus" aluminium excluded from the Al site by Ti^{3+} appears in the product assemblage as a new aluminous phase, e.g. Al_2TiO_5.

A second series of experiments was conducted to see whether Ti^{3+} would still partition into the Al-site when an excess of Al_2O_3 was present. With this aim in mind a new starting composition was prepared, "Cs-holl. mix II" equivalent to $BaAl_2Ti_6O_{16}$ (60%) + TiO_2 (30%) + Al_2O_3 (10%) plus an additional 2% Cs_2O. This was hot-pressed, first in a Ni capsule for comparative purposes, then in graphite, at temperatures ranging from 1240°C to 1290°C for one hour. Microprobe analyses and hollandite structural formulae are presented in Tables 6 and 7. In all cases, additional aluminous phases coexist with the product hollandites and rutile.

Table 6. Hot-pressing products of "Cs-holl. mix II"

T°C	1275°	1290°	1300°		1240°
HP container	Ni	graphite	graphite		graphite
			Hollandites		
TiO_2	61.0	66.9	65.5	71.9	66.3
Al_2O_3	15.6	9.4	16.7	5.4	10.6
BaO	22.5	21.5	21.9	19.7	20.9
Cs_2O	0.6	2.1	1.9	2.5	1.8
Sum	99.7	99.9	100.	99.5	99.6

Coexisting phases	rutile corundum	rutile corundum Al_2TiO_5	Ba-Ti-Al phase (analysis below)	Ba-Ti-Al phase (analysis below)
TiO_2			38.9	45.3
Al_2O_3			54.3	46.8
BaO			6.6	7.2
Cs_2O			<.2	<.2
Sum			99.8	99.3

For the sample hot-pressed in Ni, corundum is an accessory. However for samples hot-pressed in graphite, a new, uncharacterised Ba-Ti-Al phase also appears in the product assemblage (Table 6). Note that cesium does not partition into this new phase. The chemical analyses and structural formulae peculiarites of the hollandites produced by hot-pressing in graphite are again consistent with stabilization of Ti^{3+} and its entry into the Al-sites. (The Ba-Ti-Al phase may also contain Ti^{3+}). It is evident that Ti^{3+} rather than Al^{3+} preferentially enters the Al-site of hollandite, and significant partitioning of Ti^{3+} into hollandite is observed even at high Al_2O_3 activities e.g. with corundum present.

Preliminary leaching data for "Cs-holl. mix II" (Table 3) are illustrated in Fig.2. These leach-rates are similar to those obtained for "Cs-holl. mix I" composition also hot-pressed in graphite. The presence of an excess of Al_2O_3 has no significant effect on leaching performance.

Leaching data for formulations made up from the S03 hollandite preparation (Table 1) are also presented in Fig.2. Mixes corresponding to "S03 + 25% TiO_2" and "S03 + 20% TiO_2 + 5% Al_2O_3" were hot-pressed in graphite at 1200°C, and "S03 + 25% TiO_2" was likewise treated at 1300°C and subjected to leaching at 95°C (Table 8). It is evident from Fig.2 that the presence or absence of Al_2O_3 has no significant effect on leaching performance. It is also evident that the S03 preparation is intrinsically superior in its capacity to immobilize cesium, initial leach-rates bring almost one order of magnitude below those of "Cs-holl. mix I and II".

(b) Redox conditions controlled by addition of 2% metallic titanium

In many SYNROC formulations the addition of 2% Ti metal to the sample immediately prior to hot-pressing has been advocated as a means of ensuring that reducing conditions prevail during sample preparation.

Table 7. Structural formulae of hollandite produced in "Cs-holl. mix II" composition

T°C	1275°	1290°	1300°		1240°
HP container	Ni	graphite	graphite		graphite
Structural formulae based on 16 oxygen atoms					
Ti	5.722	6.383	6.234	6.869	6.280
Al	2.293	1.406	1.596	0.809	1.576
Ba	1.100	1.069	1.086	0.981	1.032
Cs	0.032	0.116	0.103	0.135	0.097
Sum	9.15	8.97	9.019	8.79	8.982
Ti + Al	8.01	7.78	7.83	7.67	7.85

Table 8. Initial Cs leach-rates for S03 hollandite preparations

Preparation	T°C	Day 1	Day 3
S03 + 25% TiO_2	1200	7.2×10^{-5}	6.7×10^{-6}
S03 + 20% TiO_2	1300	8.4×10^{-5}	6.6×10^{-6}
S03 + 20% TiO_2 + 5% Al_2O_3	1200	8.2×10^{-5}	7.2×10^{-6}

Experimental conditions: hot-pressed in Ni capsules, 1 hour at temperature shown

Table 9. Effect of Ti metal on hollandite leach-rate (gm/cm^2 day)

Hollandite preparation	Temp. ^oC	Without Ti metal		With 2% Ti metal	
		Day 1	Day 2	Day 1	Day 2
S24	1200	1.5×10^{-3}	4.7×10^{-4}	1.7×10^{-4}	1.1×10^{-4}
S24	1150	2.9×10^{-3}	3.3×10^{-4}	8.6×10^{-5}	4.7×10^{-5}
S25	1200	2.2×10^{-3}	1.5×10^{-4}	1.1×10^{-4}	5.5×10^{-5}
H1	1150	1.6×10^{-3}	7.8×10^{-5}	3.4×10^{-5}	9.9×10^{-6}
H2	"	2.3×10^{-3}	8.3×10^{-5}	3.2×10^{-5}	4.8×10^{-6}
H3	"	2.0×10^{-3}	5.1×10^{-5}	3.5×10^{-5}	7.4×10^{-6}
H4	"	1.6×10^{-3}	3.9×10^{-5}	4.6×10^{-5}	5.8×10^{-6}
S24-2A	"	7.0×10^{-5}	6.0×10^{-6}	5.6×10^{-5}	2.1×10^{-6}
S25-2A	"	1.6×10^{-4}	2.8×10^{-5}	2.5×10^{-5}	1.8×10^{-6}
S16	"	2.3×10^{-3}	1.3×10^{-4}	6.9×10^{-4}	1.6×10^{-4}
S16 + 20% TiO_2	"			1.1×10^{-3}	7.7×10^{-5}
"Cs-holl. mix I"	1200	1.4×10^{-3}	2.7×10^{-4}	1.2×10^{-4}	3.3×10^{-5}

Experimental conditions: Samples hot-pressed 1 hour in Ni capsules.

Table 10. Hot-pressing of "Cs-holl. mix I" + 2% Ti metal in Ni capsules

T°C	1350°		1325°		1300°		1250°		1200°		1150°		1100°	
	Hollandites		Hollandites		Hollandites		Hollandites		Hollandites		Hollandites		Hollandites	
TiO_2	66.1	67.6	71.4	74.4	66.7	68.4	71.6	68.1	74.4	74.0	71.1	72.1	70.5	72.2
Al_2O_3	11.1	11.1	7.1	5.7	8.4	9.0	5.8	8.1	5.8	5.9	7.0	6.1	7.1	7.3
BaO	20.7	20.6	19.8	19.7	22.1	21.7	20.3	21.5	18.7	19.4	21.0	19.9	20.0	18.9
Cs_2O	2.2	0.6	1.3	0.8	2.2	1.1	2.5	2.1	2.0	0.9	2.1	1.2	2.1	1.3
Sum	101.1	99.9	99.6	100.6	99.4	100.2	100.2	99.8	100.9	100.2	101.2	99.3	99.7	99.7
coexisting phases	rutile		rutile, Al_2TiO_5 corundum		rutile Al_2TiO_5		rutile corundum "Ti_3O_5"-type phase		rutile corundum		rutile corundum "Ti_3O_5"-type phase relict Ti metal		rutile corundum Al_2O_3-rich ss.	

Experimental conditions: Temperatures as shown above, 5 kbar, 1 hour, Ni capcaules

Table 11. Structural formulae of hollandite produced by hot-pressing "Cs-holl. mix I" + 2% metallic titanium

Based on 16 oxygens

T°C	1350°		1325°	1300°	
Ti	6.232	6.281	6.713	6.457	6.454
Al	1.640	1.616	1.046	1.274	1.331
Ba	1.017	0.997	0.970	1.115	1.069
Cs	0.118	0.032	0.069	0.121	0.059
Sum	9.007	8.927	8.799	8.967	8.910
Ti + Al	7.87	7.89	7.76	7.68	7.78

T°C	1250°		1200°		1150°		1100°	
Ti	6.814	6.523	6.891	6.874	6.705	6.816	6.686	6.725
Al	0.865	1.216	0.842	0.859	1.035	0.904	1.055	1.066
Ba	1.007	1.073	0.903	0.939	0.983	0.980	0.988	0.917
Cs	0.135	0.114	0.105	0.047	0.112	0.064	0.113	0.068
Sum	8.821	8.926	8.741	8.720	8.834	8.764	8.843	8.777
Ti + Al	7.68	7.73	7.71	7.73	7.74	7.72	7.74	7.79

Figure 3. Effect of additional 2% Ti metal on hollandite leaching performance

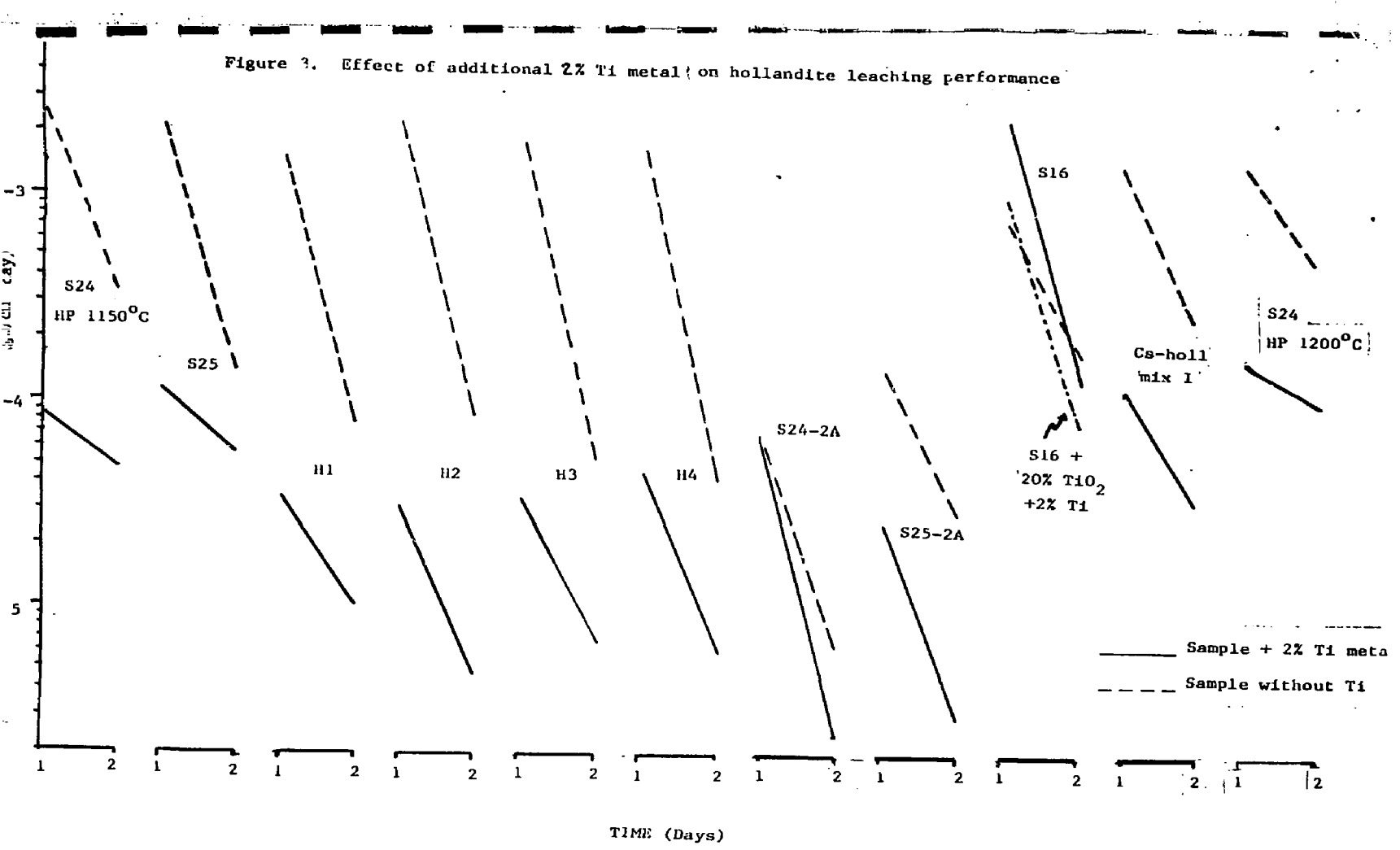

The metallic titanium serves to scavenge oxygen either from trapped air or residual nitrates, and may even scavenge nitrogen. In many cases relict Ti metal can be found mantled with TiO_2-Ti_3O_5 reaction products, indicating that (at least locally) redox conditions are sufficiently reducing so that some Ti^{3+} as well as Ti^{4+} are stable species.

The leaching performance of hollandite improves markedly if ~ 2% Ti metal is incorporated prior to hot-pressing. The ten preparations used in this study are summarized in Table 1. Table 9 and Fig.3 illustrate how Cs-based leach-rates fall by about one order of magnitude after the addition of Ti-metal, irrespective of the nature of the starting material.

Microprobe investigations again were focussed on the "Cs-holl. mix I" composition. It is evident from the microprobe analyses presented in Table 10 and the structural formulae of Table 11 that the effect of Ti metal is to lower experimental redox conditons so that Ti^{3+} is stabilized, and enters the Al-site of hollandite. As in the case where this same starting material was hot-pressed in graphite (Table 5) the hollandites exhibit an "excess" of Ti (> 6), a deficiency in Al (< 2) and an artificially low value for the sum of Ti + Al. Moreover the product assemblages contain an additional aluminous phase such as corundum or pseudobrookite (Al_2TiO_5 - Ti_3O_5 solid solutions). This is consistent with displacement of Al^{3+} from hollandite by Ti^{3+}. There is no correlation between the Cs_2O content of hollandite and its "Al-deficiency" i.e. the amount of Ti^{3+} substitution. In other words, there is unfortunately no evidence for the fixation of Cs in hollandite via the specific exchange mechanism of $2Cs^{+} + Ti^{3+}$ for $Ba^{2+} + Al^{3+}$.

(c) Leaching behaviour of S16

The leaching behaviour of hollandite preparation S16 stands out sharp contrast to the remainder of the samples in Fig.3. There is no significant difference in leaching performance when 2% Ti metal is added

to S16 alone, or to S16 + 20% TiO_2. This anomalous behaviour is believed to arise because S16 is a "stoichiometic" hollandite with molar ($BaO + Cs_2O$): (Al_2O_3): (TiO_2) = 1:1:6 with no solid solution towards the $Ba_0Al_0Ti_8O_{16}$ endmember. Reaction of Ti metal with "TiO_2" from the hollandite produces Ti^{3+}, which in turn displaces some Al from the Al-site. This reaction in effect shifts the bulk composition to molar proportions of 1: (1+x) : (6-y). Clearly this cannot crystallize as a single-phase hollandite. Any new phases which are thus stabilized may preferentially incorporate cesium and may also be relatively easily leached. This behaviour may account for the poor leaching performance of S16 + 2% Ti (Fig.3).

In principle, the addition of 20% TiO_2 to this latter composition should significantly improve its leaching performance, because there is more than enough TiO_2 to react with Ti metal, and the modification of the bulk composition as outlined above, will not occur. However as Fig.3 indicates, the leaching behaviour of S16 + 20% TiO_2 + 2% Ti is not significantly different. This disappointing result is attributed to problems arising from hand-mixing TiO_2 (anatase) with the spray-dried S16 preparation. Flocculation of anatase may have prevented satisfactory equilibration during hot-pressing, thus the problems encountered with the previous preparation were not eliminated.

5. Long-term leaching of hollandite

Ringwood et al. (1981b) reported leaching data for two hollandite preparations for periods to 60 days; by which time Cs-based leach-rates had fallen to between 5×10^{-7} and 1×10^{-6} gm/cm^2 day. Both samples had been hot-pressed in graphite and were low-Al, Ti^{3+}-bearing hollandites similar to those described in this report.

Further long-term leaching has been conducted on the Sandia Labs. preparation S25-2A, a hollandite already remarkable for a low initial leach-rate. Its leaching performance (Table 12) is illustrated in

Table 12: Long-term leaching of hollandite S25-2A

Day	leach-rate $g/cm^2 . day$
1	3.8×10^{-5}
2-3	7.1×10^{-6}
4-6	2.5×10^{-6}
7-10	1.2×10^{-6}
11-17	8.3×10^{-7}
18-27	4.7×10^{-7}
28-49	2.4×10^{-7}
50-69	2.1×10^{-7}
70-99	1.2×10^{-7}

Experimental conditions: Graphite die, 1265°C, 1 hour, 4000 psi.

Figure 4. Long-term leaching of S25-2A hollandite

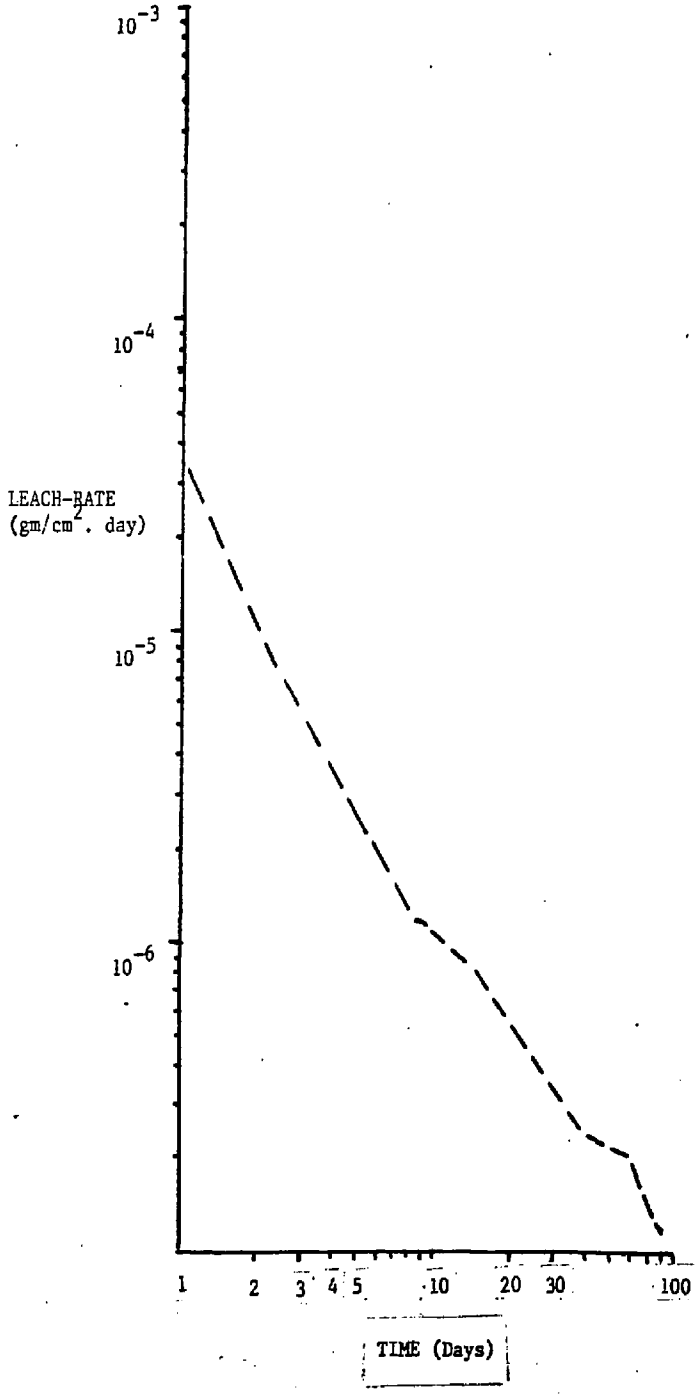

Fig.4. Note that after 80 days, its leach-rate has fallen to a new low of 1.2×10^{-7} gm/cm^2. day. So far, there is no evidence for the "plateau" reported in some of our earlier SYNROC leaching studies.

6. Conclusions

Hollandites prepared by the Sandia method exhibit superior leaching behaviour in comparison to hollandites prepared by any other technique. The leaching performance of all hollandites irrespective of preparation technique, can be markedly improved by hot-pressing under specific controlled redox conditions, below Ni-NiO. These conditions can be achieved by hot-pressing in graphite dies at modest confining pressures, or by the addition of 2% finely dispersed Ti metal powder to the sample prior to hot-pressing. For large-volume samples, the latter method will yield the best results. Hollandites produced under these conditions are characterised by an "excess" of TiO_2 and a "deficiency" in Al_2O_3. In effect, Ti^{3+} stabilized at these ambient low oxygen fugacities, preferentially partitions into the Al-site, displacing Al^{3+} into new aluminous phases such as corundum or pseudobrookite.

There is no satisfactory crystal-chemical reason why the leaching performance of Ti^{3+}-bearing hollandite should be superior to that of Al^{3+} hollandite. The most likely explanation is that there are kinetic factors involved and reaction pathways may be different when Ti^{3+} is present, since the activity of $(Ti + Al)^{3+}$ is necessarily higher in these cases. Metastable Cs-bearing phases formed prior to or during hollandite nucleation may not be completely eliminated unless Ti^{3+} is present in the system. These relict metastable phases may contribute to poor Cs leach-rates in hollandite formulations hot-pressed in Ni, and without additional Ti metal.

7. References:

Oversby, V.M. and Ringwood, A.E. (1980). Leach-testing of SYNROC and glass samples at 85°C and 200°C. Nucl. Chem. Waste Manage-

ment, in press.

Ringwood, A.E., Oversby, V.M. and Kesson, S.E. (1981a). Experiments bearing on the optimum preparation and heat-treatment of SYNROC formulations, with implications for the fixation of cesium and molybdenum. Unpublished report.

Ringwood, A.E., Oversby, V.M., Kesson, S.E., Sinclair, W., Ware, N., Hibberson, W. and Major, A. (1981b). Immobilization of high level nuclear reactor wastes in SYNROC; A current appraisal. ANU publication 1475. Submitted to Nucl. Chem. Waste Management.

Incorporation of Uranium and Rare Earths into Zirconolite

S. Kesson and A.E. Ringwood

Research School of Earth Sciences
Australian National University
Canberra, A.C.T. 2600, Australia

1. Introduction

The rare earths and trivalent and tetravalent actinides are immobilized in SYNROC by two phases, zirconolite and perovskite. A reconnaissance experimental study has been undertaken to explore the tolerance of the zirconolite lattice to substitutions involving the above elements, since high concentrations of actinides or rare earths may tend to stabilize a less-desirable pyrochlore phase in preference to zirconolite. The experiments were specifically aimed at determining how much uranium, and samarium or neodymium could be accommodated in the zirconolite lattice before it was destabilized in favour of pyrochlore. Here, uranium serves as a model for all tetravalent actinides and the rare earths also model the behaviour of the trivalent actinides. Naturally-occurring zirconolites contain as much as 23 wt.% ThO_2 + UO_2 and up to 9% rare earths (REE). Sinclair and Ringwood (1981) have shown that these samples, which are now metamict, recrystallize to recover their zirconolite structure after heat-treatment at $\sim$1100°C.

2. Paragenesis of Zirconolite

Zirconolite occurs in trace amounts in a variety of environments and is usually found as small grains up to several millimeters in dimension. At Jacupiranga, Brazil, it occurs in the magnetite-pyroxenite rock which intrudes the carbonatite complex (Hussak and Prior, 1895). In Germany, zirconolite has been found in several dikes which intrude the Kaiserstuhl carbonatite (Keller, pers. comm.).

The mineral has been reported in several locations in the USSR (Vlasov, 1966). Samples from Arbarastakh in Aldan are contained in the central regions of pyroxenite massifs. The

pyroxenites outcrop in a group of ultrabasic alkali rocks and have been subjected to intense metasomatic alteration (Borodin et al., 1960). A niobium-rich variety of zirconolite from the apatite-magnetite rocks of the Vuoriyarvi massif has also been reported by these authors. Zirconolite from the Kola Peninsula occurs in the coarse grained pyroxene-amphibole rock of the Afrikanda massif.

In Sri Lanka, zirconolite occurs as large pebbles weighing up to 60 grams. They are found in gem gravels at several localities (Blake and Smith, 1913).

The oldest known specimens on earth have been found in the Jimberlana Intrusion, Western Australia. The intrusion consists of a layered horizontal mafic complex and has been dated at about 2500 m.y. old (Turek, 1966; Oversby and Ringwood, 1980). Recently, Williams (1978) has reported an occurrence of zirconolite in the Rhum ultrabasic layered intrusion. The zirconolite is interpreted to be a late stage mineral containing the remaining incompatible elements of the original magma.

Samples from Norway are known as polymignite (Palache et al., 1944; Vlasov, 1966). This mineral is found in Norway in a pegmatite with Na-orthoclase, magnetite, nepheline, zircon and pyrochlore. It has also been found in augite-syenite rocks.

3. Crystal Chemistry of Zirconolite

The crystal structure of zirconolite has been described in detail by Rossell (1980a) and Gatehouse et al. (1981). They confirmed earlier work by Pyatenko and Pudovinka (1961) by showing that it is related to structures of the defect fluorite-type, in that it is a superst ucture derived by ordering of CaF_{2-x} type sub-units. The c-c ntred monoclinic unit cell of zirconolite is eight times as large as the fluorite-type sub-unit, and its structure is more correctly expressed by the formula $Ca_8Zr_8Ti_{16}O_{56}\square_8$ ($\square$ symbolises an oxygen vacancy).

Rossell (1980a) found that the Ca atoms are coordinated to 8 oxygens at the corners of a distorted cube. Zirconium, in seven-fold coordination, is linked to 7 oxygens at the corners of a truncated cube. Titanium occupies three distinct lattice sites. In two of these, it is in 6-fold coordination, linked to

Fig. 1. The system $CaZrTi_2O_7$ - "$CaTi_3O_7$" - $CaZr_2TiO_7$.

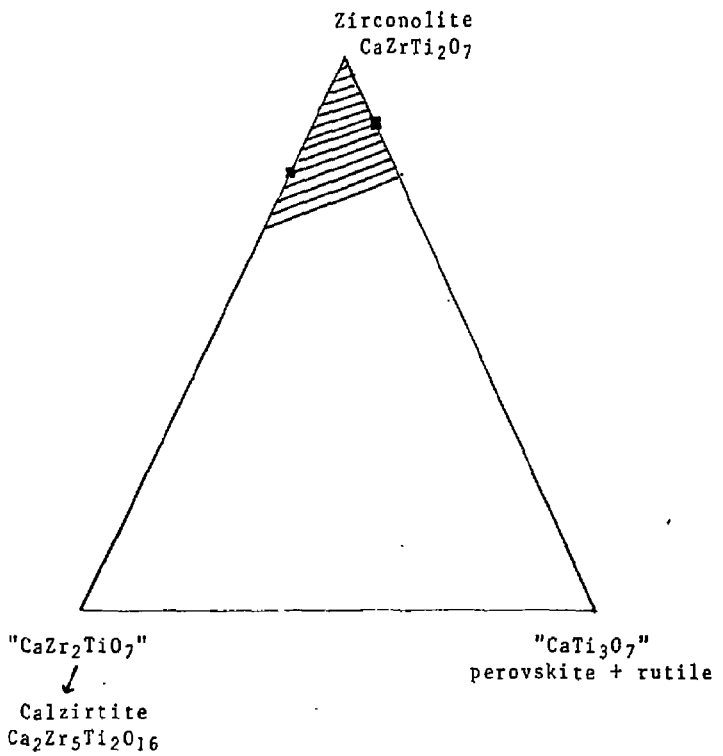

Shaded field shows limits of zirconolite solid solution towards calzirtite and "$CaTi_3O_7$" as defined by Gatehouse et al. (1980). Solid squares indicate compositions synthesised at 1350°C and 1400°C at ANU.

6 oxygens at the vertices of octahedra. These octahedra are linked at their corners, forming either 6-membered or 3-membered rings. The third type of titanium site involves 5-fold coordination with titanium linked to 5 oxygens at the apices of a trigonal bipyramid.

Crystal-chemical studies of zirconolite by Gatehouse et al. (1981) have defined the compositional range of zirconolite. They also showed that the lattice parameters range systematically as a function of composition and temperature. They found that zirconolite was remarkably intolerant to variations in its Ca content, permitting changes of only a few atom %. However, considerable variation in Zr/Ti ratios is permitted. If the formula of zirconolite is written as $CaZr_xTi_{3-x}O_7$ then x ranges from 0.9 to 1.3. In other words, zirconolite exhibits solid solutions towards two other components, namely $Ca_2Zr_5Ti_2O_{16}$ (calzirtite) and "$CaTi_3O_7$" (Fig. 1). Experiments in our laboratory have confirmed that at 1350°C, zirconolite solid solutions with up to 10 mole % of "$CaTi_3O_7$" are stable. This is relevant to SYNROC formulations where zirconolite coexists with $CaTiO_3$ ± rutile at similar temperatures. Similar experiments have established that solid solutions with 18 mole % $CaZr_2TiO_7$ component can be synthesized at 1400°C. These results are shown in Figure 1.

Natural and synthetic zirconolites have been found to accommodate a wide range of cation substitutions. In order to facilitate discussion of the crystal chemistry we will simply describe cation substitutions in terms of the Ca- Zr- or Ti-sites. Table 1 presents microprobe analyses of a suite of natural zirconolites from many countries. Of particular relevance to radwaste immobilization is the observation that natural zirconolites may contain as much as 23 wt.% ThO_2 plus UO_2, and 9 wt.% rare earth elements (Table 1). Because many natural zirconolites are metamict, the distribution of cations amongst the various sites cannot be resolved by conventional X-ray techniques. However, the structural formulae of the natural samples (Table 1) when coupled with crystal chemical considerations, are quite revealing. The 8-fold coordinated Ca-site should be particularly suited for large cations e.g. Ca^{2+}, U^{4+}, Th^{4+} and the larger rare earths. The 7-fold coordinated Zr-site would best be occupied by Zr^{4+}, some

Table 1. Chemical analyses of natural ZIRCONOLITES.

Locality	Stavern (Brown)	Stavern (Red)	Larvik	Jacupiranga	Aldan	Kaiserstuhl	Sri Lanka (B20392)	Sri Lanka (83800)	Sri Lanka (SL3-12)
Nb_2O_5	18.9	15.6	8.0	11.3	4.6	15.6	3.6	3.9	<0.2
Ta_2O_5	0.4	<0.2	0.7	0.2	<0.1	1.2	-	-	<0.1
TiO_2	16.7	22.4	27.0	24.3	35.4	20.9	28.0	27.0	36.5
ZrO_2	32.0	35.3	31.4	35.2	36.5	34.8	30.9	30.4	38.6
ThO_2	3.7	0.6	4.1	7.4	1.2	2.9	20.5	21.8	0.9
UO_2	1.9	0.3	1.3	0.5	0.5	1.5	2.1	1.7	4.6
FeO*	9.3	8.4	6.9	7.2	5.0	7.8	3.1	3.0	3.4
MnO	.5	0.4	0.5	0.2	<0.1	0.2	-	0.2	0.2
MgO	-	-	-	0.4	-	0.3	2.4	2.5	0.6
CaO	7.7	10.0	9.2	11.5	15.1	12.1	7.9	7.7	12.1
REE,Y	6.6	4.8	9.3	2.6	1.9	0.9	-	-	-
Sum	97.7	97.8	98.4	100.8	99.2	98.2	98.5	97.2	96.9

Electron microprobe analyses by N.G. Ware, except data for Larvik (A. Råheim, pers. comm.). *All iron assumed to be FeO.

Structural formulae based on 7 oxygen atoms

Nb	0.596	0.463	0.243	0.332	0.126	0.464	0.113	0.125	-
Ta	0.008	-	0.013	0.004	-	0.022	-	-	-
Ti	0.876	1.105	1.366	1.186	1.611	1.034	1.456	1.433	1.718
Zr	1.089	1.129	1.030	1.114	1.077	1.117	1.042	1.047	1.178
Th	0.059	0.009	0.063	0.109	0.003	0.043	0.323	0.350	0.013
U	0.030	0.004	0.020	0.007	0.006	0.022	0.032	0.027	0.064
Fe"	0.543	0.461	0.388	0.391	0.253	0.429	0.179	0.118	0.178
Mn	0.030	0.022	0.029	0.011	-	0.011	-	0.012	0.011
Mg	-	-	-	0.039	-	0.029	0.247	0.263	0.056
Ca	0.576	0.703	0.663	0.800	0.978	0.853	0.585	0.582	0.811
REE,Y	0.159	0.109	0.216	0.058	0.040	0.020	-	-	-
Sum	3.963	4.004	4.030	4.051	4.094	4.045	3.978	3.957	4.028

Ti^{4+} and the smaller rare earths. In section 4 of this paper we present evidence for the somewhat unexpected substitution of U^{4+} into this site. The Ti-sites, in 6- and 5-fold coordination, should be particularly suited for small cations such as Ti^{4+}, Nb^{5+}, Ta^{5+}, Mg^{2+}, Mn^{2+}, Fe^{2+}, Fe^{3+} and minor Zr^{4+}.

Inspection of the structural formulae of the natural samples (Table 1) reveals some interesting trends. With one exception (Aldan), full occupancy of the Ca-site requires significant amounts of other cations as well as calcium. Even if all the available Th and U is then allocated to the Ca-site, it is still not fully occupied. Small amounts of rare earths are also required. Note that even if all rare earths were fully partitioned into the Ca site, some U and Th are nevertheless required for full occupancy. As discussed above, the Zr site can contain small amounts of Ti, whilst small amounts of Zr may partition into the Ti-sites. Whilst we cannot deduce the exact nature of this partitioning from the structural formulae, it is nevertheless significant that all samples contain in excess of 1.00 Zr atoms and in many cases, the amounts of Nb, Ta, Mg, Mn, Fe and Ti are insufficient to fill the two Ti-sites completely. It follows that a significant proportion of Zr must be partitioned into the Ti sites. The above constraints on site occupancy also lead to the conclusion that most Th and U is concentrated in the Ca-site, with very little being partitioned into the Zr-site. In a study of synthetic zirconolites, Rossell (1980b) came to a similar conclusion.

Zirconolites which crystallize in SYNROC formulations aimed at immobilizing US defense wastes contain significant amounts of other elements such as Mn, Fe, Al and minor amounts of Na and Ni. Iron is probably present as both divalent and trivalent cations, so there are uncertainties introduced in the derivation of structural formulae from microprobe analyses where iron is automatically calculated as "FeO". However, some trends are significant - a covariance between CaO and MnO suggests Mn^{2+} is strongly partitioned into the Ca-site. Strontium is most reluctant to enter zirconolite under any circumstances, indicating that the Ca-site cannot readily accommodate ions much larger than Ca^{2+}, whereas smaller species (e.g. Mn^{2+}) fit comfortably. Nickel contents of zirconolites are invariably low (typically less than 0.5%) suggesting that the octahedrally-coordinated Ti-sites are suitable only

for smaller cation species. The site occupancy of iron is uncertain, but it seems reasonable to believe it could occupy both Zr- and Ti-sites. The preferred site occupancy of certain key elements such as Mg, Fe, Co, Ti and rare earths should soon be confirmed by the results of a detailed study presently being carried out by Rossell (pers. comm.).

4. Incorporation of Uranium into Zirconolite

The solid solution limits between $CaZrTi_2O_7$ (zirconolite) and $CaUTi_2O_7$ (pyrochlore) were explored in order to establish how much substitution of zirconium by uranium could be tolerated by the zirconolite structure before it was destabilized in favour of pyrochlore. Compositions corresponding to $CaZr_{.25}U_{.75}Ti_2O_7$, $CaZr_{.5}U_{.5}Ti_2O_7$ and $CaZr_{.75}U_{.25}Ti_2O_7$ were hot-pressed at 1400°C. Trace amounts of $(Zr,Ti,U)O_2$ solid solutions were observed in all runs. Homogeneous pyrochlore phases were synthesized from the first two starting materials. Product assemblages were studied by X-ray diffraction and electronprobe microanalysis. The $CaZr_{.75}U_{.25}Ti_2O_7$ preparation yielded a pyrochlore + zirconolite assemblage. The compositions and structural formulae of this pair are given in Table 2. Rossell (1980b) has argued that the entry of Th (and by implication, U) into the zirconolite lattice involves its partition into the Ca site, with coupled substitution of a lower-valency ion (e.g. Ti^{3+}) into the Zr site. Whilst this may well have occurred in his experiments, we find no evidence for substitution mechanisms of this kind in our own experiments. The structural formulae in Table 2 indicate that the entry of uranium into the zirconolite lattice is via a simple substitution. U^{4+} proxies primarily for Zr^{4+}, with a very small amount also being partitioned into the Ti sites. The UO_2 content of this zirconolite is 13%. This type of behaviour has been observed many times in other SYNROC formulations.

It is possible that the entry of U^{4+} into the Ca-site might be facilitated by a coupled substitution whereby U^{4+} replaces Ca^{2+} and a lower-valence cation (e.g. Mg^{2+}) substitutes for Ti^{4+}. To this end, we investigated the solid solution limits between U-bearing zirconolite and pyrochlore and the hypothetical end-member "$UZrTiMgO_7$". The product assemblages contained various $(Ti,Zr,U)O_2$ solid solutions and some uncharacterized phases,

Table 2. Coexisting pyrochlore and zirconolite synthesized from $CaU_{.25}Zr_{.75}Ti_2O_7$.

	Zirconolite	Pyrochlore
TiO_2	42.3	37.3
ZrO_2	29.1	18.9
UO_2	12.6	28.0
CaO	15.2	15.7
Sum	99.2	99.9

Structural formulae based on 7 oxygen atoms.

Ti	1.955	1.891
Zr	0.872	0.621
U	0.172	0.420
Ca	1.001	1.134
Sum	4.001	4.067

Zirconolite
Model molecule: $Ca_{1.00}(U,Zr)_{1.00}(Ti,Zr)_{2.00}O_7$

Starting composition: $CaU_{.25}Zr_{.75}Ti_2O_7$

Experimental conditions: 5 kbar, 1400°C, 1 hr., Pt capsule.

however, one phase, with a very narrow composition range, was common to all product assemblages. Its composition range and structural formula are presented in Table 3. X-ray diffraction established that this phase is a zirconolite. Note how the entry of Mg into the lattice has permitted substitution of additional U^{4+}. The UO_2 content of this zirconolite (~26%) is substantially higher than that (13%) of the Mg-free zirconolite in Table 2. The structural formulae and "model molecules" calculated on the basis of our analytical data confirm that additional U^{4+} can be persuaded to enter the Ca-site of the zirconolite lattice by means of a coupled substitution involving Mg^{2+} entering the Ti-sites.

Rossell (1980b) has proposed that Ti^{3+} (or Mg^{2+}) enter the Zr-site, thereby allowing Th^{4+} (and hence U^{4+}) to enter the Ca-site. We find it difficult to accept that Ti^{3+} was a stable species in his experiments, since most of these apparently involved synthesis in air. (Other work in our laboratory finds evidence for Ti^{3+} only when oxygen fugacity conditions are very low indeed, below the Fe-FeO buffer). Moreover, we suspect that small cations would prefer the 5- and 6-fold coordinated Ti-sites. However, Rossell's data are actually reasonably consistent with our own preferred interpretation of site occupancies, namely that (Ca,U) (Zr,U,Ti) and (Ti,Mg,Zr) respectively occupy the Ca, Zr, and Ti-sites of zirconolite. All the Ti in the Zr-site is in the 4+ state; there is no evidence to suggest that Ti^{3+} is stabilized.

In Section 3 we concluded that in natural zirconolites a significant proportion of uranium was located in the Ca-site. This probably reflects a coupled substitution of the above type, involving Mn^{2+}, Fe^{2+} and Fe^{3+} as well as Mg^{2+}.

5. Incorporation of Rare Earths into the Zirconolite Lattice

A starting mixture with composition corresponding to 1:1 molar $CaZrTi_2O_7$ and $NdYTi_2O_7$ was hot-pressed at 1500°C for 1 hr. Neodymium and yttrium are similar in size to calcium and zirconium respectively and so it was anticipated that the zirconolite lattice would be especially tolerant to the coupled substitution of Nd + Y for Ca and Zr (yttrium behaves as an excellent crystal-chemical

Table 3. Mg-bearing U-rich zirconolites.

TiO_2	33.4	34.6
ZrO_2	25.1	25.1
UO_2	26.8	25.1
MgO	1.6	2.4
CaO	13.2	12.8
Sum	100.1	100.0

Structural formulae based on 7 oxygen atoms

Ti	1.704	1.735
Zr	0.831	0.816
U	0.405	0.372
Mg	0.162	0.239
Ca	0.960	0.915
Sum	4.061	4.077

Model molecules[1] $(Ca,U)_{1.00}(Zr,U)_{1.00}(Ti,Mg,Zr)_{2.06}O_7$
$(Ca,U)_{1.00}(Zr,U)_{1.00}(Ti,Mg,Zr)_{2.08}O_7$

Experimental conditions: 5 kbar, 1400°C, 1 hr., Pt capsule.

Starting compositions: $Ca(Zr,U)Ti_2O_7$ ss. + "$UZrMgTiO_7$"

[1]Calculated by filling Ca-site with Ca+U, then filling Zr-site with Zr+U. Residual Zr plus Mg and Ti are allocated to Ti-sites.

analogue for the heavy rare earths). However, the experimental product turned out to be a homogeneous single-phase pyrochlore solid solution whose composition is given in Column 1, Table 4.

A second composition corresponding to a 1:1 molar mixture of two end-member phases, $CaZrTi_2O_7$ and $Sm_2Ti_2O_5$ was hot-pressed at 1400°C and 1450°C. In this instance, a pair of coexisting phases (low-Zr and high-Zr phases of Table 2) were produced. Subsequent synthesis of these two phases confirmed that the low-Zr phase is a pyrochlore, whilst the high-Zr phase is a zirconolite. (The composition of the newly-synthesized high-Zr phase is given under "C" in Table 4. Note the high rare earth content of 27% Sm_2O_3). However, because the starting material consisted of a mixture of two previously-synthesized end-members, we recognised the possibility that the coexisting pyrochlore-zirconolite pair might be metastable with respect to a homogeneous single phase. This was confirmed when a new starting mix of oxides + carbonates corresponding to the appropriate composition was hot-pressed at 1450°C and a single phase pyrochlore-type (f.c.c.) solid solution was produced.

6. Conclusions

Electron microprobe analyses of a suite of natural zirconolites reveal that Nb, Ta, Th, U, Fe, Mn, Mg, Y and rare earths can be accommodated in the zirconolite lattice. Many of the natural samples are metamict but have recrystallized to single-phase zirconolite after heat treatment (Sinclair and Ringwood, 1981). In SYNROC formulations, and along the binary join $CaZrTi_2O_7$-$CaUTi_2O_7$, entry of U into the zirconolite lattice essentially involves substitution in the Zr-site. Natural zirconolites, on the other hand, appear to accommodate significant amounts of U in the 8-fold coordinated Ca-site. Presumably, in chemically-complex natural minerals, this substitution is facilitated by entry of small, lower valence cations into the Ti-sites e.g. Al^{3+}, Fe^{3+}. Laboratory experiments have confirmed that the entry of U into the Ca-site is facilitated by a coupled substitution whereby a small divalent cations such as Mg^{2+} is simultaneously partitioned into the Ti-sites. Natural zirconolites may contain up to 23% $ThO_2 + UO_2$; synthetic zirconolites along the $CaZrTi_2O_7$ - $CaUTi_2O_7$ join take up only ~13% UO_2. (At higher UO_2 contents a pyrochlore phase is preferentially stabilized). However, when coupled substitutions

Table 4. Rare earth-bearing pyrochlores and zirconolite.

	A	B		C	D
		Low Zr-phase	High-Zr phase	High Zr-phase	
TiO_2	40.8	38.4	40.0	40.5	37.6
ZrO_2	16.0	14.0	22.0	24.9	16.3
Sm_2O_3	-	40.5	29.4	26.5	38.5
Nd_2O_3	21.5	-	-	-	-
Y_2O_3	14.	-	-	-	-
MgO*	0.4	0.8	0.6	-	SrO=0.4
CaO	7.2	6.1	7.7	8.5	7.2
Sum	99.9	99.8	99.9	100.4	100.0
Structure:	pyrochlore	pyrochlore	zirconolite	zirconolite	pyrochlore-type

Structural formula based on 7 oxygens:

Ti	1.974
Zr	0.787
Sm	0.592
Ca	0.590
Sum	3.943

Starting composition: A = $CaZrTi_2O_7$ + $NdYTi_2O_7$ 1:1 molar

B = $CaZrTi_2O_7$ + $Sm_2Ti_2O_7$ 1:1 molar mixture of the two components

C = High-Zr phase from "B"

D = $CaZrTi_2O_7$ + $Sm_2Ti_2O_7$ oxide/carbonate mix.

Experimental conditions: 5 kbar, 1450°C, 1 hr., Pt capsule.

involving Mg takes place, UO_2 contents of 27% can be achieved.

SYNROC formulations developed for immobilizing civilian high-level wastes typically comprise about 35 wt.% zirconolite. Waste-loadings may be as high as 20% and the calcined waste itself contains about 1% UO_2. From these constraints we deduce that the zirconolite will be required to accommodate only about 0.6% UO_2, and will be way below its "saturation limit". The situation is somewhat different in the case of SYNROC formulations designed to immobilize the iron and alumina-rich sludges resulting from the US Defense program. These calcined sludges contain quite high concentrations of UO_2 ($\sim$3%). Moreover, the waste-loading of SYNROC is now much higher ($\sim$65%) and the wasteform itself contains a smaller proportion of zirconolite ($\sim$13%). It follows that the zirconolite phase will be required to immobilize about 15 wt.% UO_2. If this uranium were to be accommodated by simple substitution into the Zr-site, the zirconolite phase would be dangerously close to the "saturation limit". However, the high concentrations of iron, aluminium etc. in the Defense sludges give rise to zirconolites which themselves contain significant amounts of these elements. The zirconolite is thus able to accommodate additional uranium via the coupled substitution mechanism discussed earlier, and is still well below its "saturation limit" with respect to uranium and tetravalent actinides.

Natural zirconolites may contain at least as much as 9% rare earths. Zirconolites in SYNROC formulations will be required to accommodate only a few percent of rare earths and trivalent actinides. Experiments have shown that the zirconolite lattice can accept up to 30% rare earths (Sm_2O_3) before becoming destabilized in favour of pyrochlore or a related f.c.c. structure. SYNROC zirconolites will therefore be well below their "saturation limits" in rare earths and trivalent actinides.

7. References

Blake, G.S. and Smith, G.F.H. (1913) On varieties of zirkelite from Ceylon. Mineral. Mag. 16, 309-316.

Borodin, L.S., Bykova, A.B., Kapitonova, T.A. and Pyatenko, Y.A. (1960) New data on zirconolite and its niobian variety. Akad. Nauk. SSSR 134, 1188-1191.

Gatehouse, B.M., Grey, I.E., Hill, R.J. and Rossell, H.J. (1981) Zirconolite, $CaZr_xTi_{3-x}O_7$: structure refinements for near end-member compositions with x = 0.85 and 1.30. Acta Krist., in press.

Hussak, E. and Prior, G.T. (1895) Lewisite and zirkelite, two new Brazilian minerals. Mineral. Mag. 11, 80-88.

Oversby, V.M. and Ringwood, A.E. (1981) Lead isotopic studies: zirconolite and perovskite and their implications for long range SYNROC stability. Radioactive Waste Management, in press.

Palache, C., Berman, H. and Frondel, C. (1944) (Eds.) "The System of Mineralogy of J.D. Dana and E.S. Dana". 7th Edition. John Wiley and Sons, New York, 834 p.

Pyatenko, Y.A. and Pudovinka, Z. (1961) The crystal structure of calzirtite: a new derivative structure of CaF_2-CeO_2 type. Kristallografiya 6, 196-199.

Rossell, H.J. (1980a) Zirconolite - a fluorite-related superstructure. Nature 283, -82-283.

Rossell, H.J. (1980b) A crystal-chemical study of non-stoichiometric and alloyed zirconolites. Manuscript in preparation.

Sinclair, W.S. and Ringwood, A.E. (1981) Effects of nuclear radiation on the crystal structures of zirconolite and perovskite. Geochem. Journal, in press.

Turek, A. (1966) Rb-Sr isotopic studies in the Kalgoorlie-Norseman area, Western Australia. Australian National University, Ph.D. Thesis.

Vlasov, K.A. (ed.) (1966) Geochemistry and Mineralogy of Rare Elements and Genetic Types of their Deposits. Israel Program for Scientific Translations. Vol. 2, Jerusalem.

RECONNAISSANCE STUDIES OF THE STABILITY RELATIONS OF Ca-Ti-Al PHASES IN SYNROC-C FORMULATIONS

S.E. Kesson and A.E. Ringwood

1. Introduction

Ca-Ti-Al bearing phases have been observed in many SYNROC-C preparations. X-ray data indicate two distinct structural types (i) a previously uncharacterised Ca-Ti-Al phase (CTA) with the composition $CaTi_3Al_8O_{19}$ and (ii) Fe,Ti-bearing calcium aluminate phases with the magnetoplumbite structure. A reconnaissance experimental program has been undertaken in order to characterise these phases and to elucidate their stability relations in SYNROC-C formulations.

The interpretation of experimental assemblages in this program was beset by many difficulties. For example, corundum and perovskite, once nucleated, are notoriously reluctant to react again outside their stability fields. Secondly, in many simple systems (e.g. Al_2O_3-TiO_2-CaO), melting occurred, as evidenced by abrupt textural changes (e.g. development of euhedral phenocrysts). The liquid always quenched to a multiphase crystalline matrix, and so it follows that phenocryst + matrix phases do not necessarily represent an equilibrium assemblage. Finally, the interpretation of subsolidus experiments was hampered by the fine grain size of the products, making microprobe analysis very difficult.

Further difficulties were encountered as a result of the preparation of acceptable starting materials. Oxide mixtures proved less reactive and less homogeneous than nitrate ± carbonate mixtures, hence relict unreacted corundum, for example, might be found amongst the products. However, whilst nitrate ± carbonate starting materials were more reactive and very homogeneous, they sometimes contained traces of residual nitrates, which acted as fluxes during high-pressure experiments and catalysed melting and breakdown reactions at lowered temperatures. This handicapped the systematization of phase assemblages as a function of temperature.

2. Characterization of $CaTi_3Al_8O_{19}$

Microprobe analyses of CTA phases in iron-free SYNROC-C formulations showed a narrow composition range, essentially $CaTi_3Al_8O_{19}$.

An attempt to prepare the pure phase from an oxide mixture of this composition was successful after several iterations of grinding and repelletizing at 1300°C. Powder diffraction X-ray data were obtained for this new phase and are listed in Table 2. Clearly, $CaTi_3Al_8O_{19}$ is not isostructural phases such as hibonite $CaAl_{12}O_{19}$, which possess the magnetoplumbite structure.

3. Partition of radwaste elements into CTA

The partition behaviour of key elements into CTA has been elucidated by electronprobe analysis. The study included both SYNROC-C formulations and simple two-phase assemblages involving CTA and individual SYNROC phases. Neither BaO nor ZrO_2 show any particular preference for $CaTi_3Al_8O_{19}$, abundances of 0.2% being typical. UO_2 and Cs_2O are normally below detection limits. Nickel shows a marked preference for hollandite rather than $CaTi_3Al_8O_{19}$, rarely exceeding 0.5% NiO. Ferric iron is able to substitute readily for Al^{3+}, but its solubility limits have not been explored. In perovskite-free SYNROC formulations, several percent of SrO is readily accepted by this new phase, thus providing the option of its substituting for perovskite as a host for Sr in SYNROC assemblages. An isostructural phase corresponding to $Ca_{.5}Sr_{.5}Ti_3Al_8O_{19}$ (i.e. 7% SrO) was successfully synthesised at 1320°C and 5 kbar. Small percentages of rare earths have been detected in $CaTi_3Al_8O_{19}$, however, partition experiments show that perovskite and zirconolite remain the major REE hosts.

4. Leaching of Sr-bearing CTA

At 200°C, in pure water, $Ca_{.5}Sr_{.5}Ti_3Al_8O_{19}$ proved very similar to perovskite in terms of Sr leachability (Oversby and Ringwood, 1980). It follows that the capacity of SYNROC to immobilize strontium would be essentially unchanged, if $CaTi_3Al_8O_{19}$ were to replace perovskite in specific SYNROC-C formulations.

5. Stability relations of $CaTi_3Al_8O_{19}$

(a) Melting behaviour

Experiments at 5 kbar established that at 1450°C, $CaTi_3Al_8O_{19}$ melted incongruently producing phenocrysts of a new

Table 1.

CTA phase (mean of 8 analyses)

TiO_2	34.1
Al_2O_3	57.7
CaO	8.2
Sum	100.0

Molecular proportions based on 19 oxygens

Ti	3.005
Al	7.976
Ca	1.026
Sum	12.007

Structural formula $CaTi_3Al_8O_{19}$

Starting composition: TiO_2 = 35.9, Al_2O_3 = 55.7, CaO = 8.5

Experimental conditions: 5 kbar, 1350°C, 1 hr, Pt caps.

Product assemblage: Texture suggests melting. Euhedral megacrysts of CTA in fine groundmass of perovskite + corundum.

Table 2. Characteristic of spacings (Å) of $CaTi_3Al_8O_{19}$

dÅ	I
5.6	w
3.79	wm
3.123	w
2.845	s
2.777	w
2.739	w
2.649	wm(b)
2.555	w
2.499	w
2.441	w
2.383	ms
2.267	w
2.182	wm
2.145	m
2.092	ms
1.984	w
1.950	w
1.894	m
1.757	wm
1.738	w
1.636	w
1.609	w
1.601	w
1.528	m
1.509	w(b)
1.436	wm
1.420	m
1.402	ms
1.383	mb

s = strong
m = medium
w = weak
b = broad

uncharacterized CTA phase (essentially $Ca_4Al_2Ti_8O_{23}$) in a fine matrix of corundum, perovskite and rutile. The liquidus was not determined accurately but is believed to lie around 1500°C.

(b) Phase compatibilities in the system Al_2O_3-TiO_2-CaO

Our experimental study of this system was confined to the area bounded by corundum (Al_2O_3), rutile (TiO_2) and perovskite ($CaTiO_3$). Pseudobrookite (Al_2TiO_5) and CTA ($CaTi_3Al_8O_{19}$) are also contained in this field (Fig. 1). Table 3 summarised the experiments which define the phase relationships and establish the progressive sequence of reactions as a function of increasing temperature. As mentioned in the introduction, certain difficulties beset the interpretation of experimental results.

The first eight experiments establish the 3-phase field CTA-perovskite-corundum over a temperature range from 1350 to 1500°C. Note that at 1500°C, CTA is replaced by its incongruent melting product (Exp. 5). Experiments 9-11 establish the coexistence of CTA, pseudobrookite and corundum. Despite incomplete reaction in #12, the product assemblage is highly significant because it establishes that under subsolidus conditions, the join CTA-rutile is stable. Subsolidus compatibility relations in the system are illustrated in Figure 2a. Note that perovskite and pseudobrookite are not permitted to coexist at temperatures around 1300°C. Experiments 13 and 14 show that the join CTA-rutile has been broken, and offer two possible interpretations. The first case is shown in Figure 2b, where a condensed-phase reaction has taken place just below the solidus, with CTA and rutile reacting to yield perovskite + pseudobrookite. The CTA-rutile join disappears and perovskite-pseudobrookite are permitted to coexist. An alternative scenario is presented in Figure 2c. Here, the solidus has been intersected and the small liquid field breaks the CTA-rutile join. The presence of the liquid field also prohibits the coexistence of perovskite and pseudobrookite. (This latter interpretation is preferred, because in SYNROC formulations, perovskite and pseudobrookite are virtually never observed together). The join between CTA and perovskite is probably also cut by the liquid field at these temperatures. The ceramics literature shows that the liquid field breaks the perovskite-rutile join at ~1460°C and our own experiments, which show that CTA has begun to melt by 1450°C,

Fig. 1. Phases in the system Al_2O_3-TiO_2-CaO

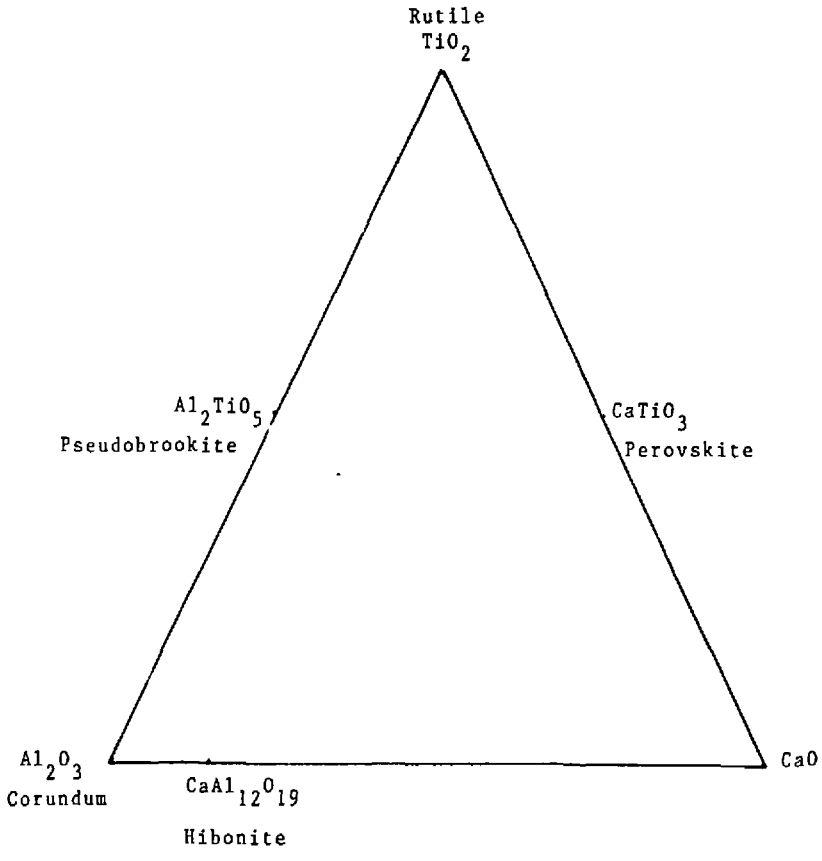

The following phases are not plotted on the diagram:

$3CaO.2TiO_2$

$4CaO.3TiO_2$

$3CaO.Al_2O_3$

$12CaO.2Al_2O_3$

$5CaO.3Al_2O_3$

$CaO.Al_2O_3$

$CaO.2Al_2O_3$

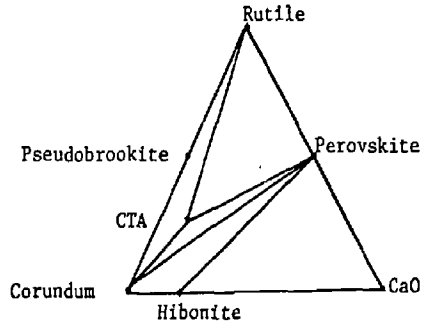

CTA = $CaTi_3Al_8O_{19}$

▨ = liquid field (tie-lines not shown)

(a) Subsolidus compatibility fields ∿1300°C.

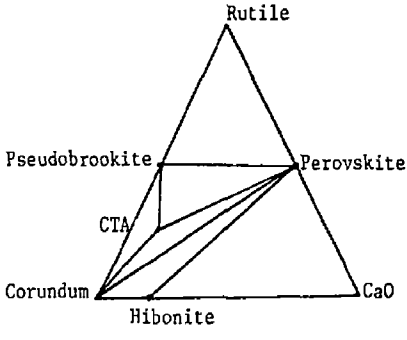

EITHER (b) CTA + rutile + perovskite + pseudobrookite

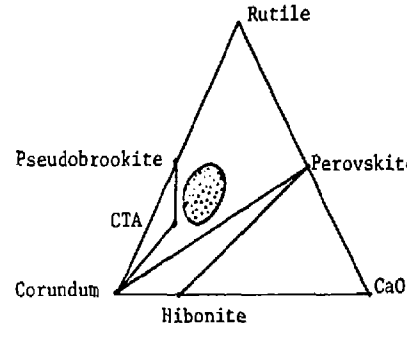

OR (c) Melting begins 1300-1400°C.

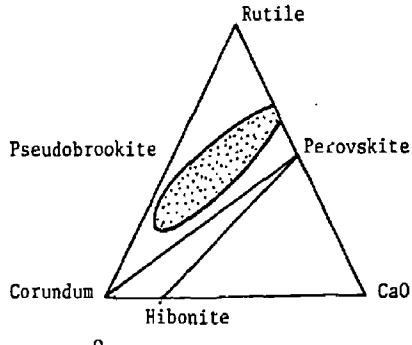

(d) By ∿1500°C liquid field eliminates CTA (and any incongruent melting products) breaks rutile-perovskite join.

(e) By ∿1900°C, liquid field eliminates pseudobrookite, perovskite rutile and hibonite.

Fig. 2. Progressive reactions in the system Al_2O_3-TiO_2-CaO with increasing temperature.

Table 3. Phase assemblages produced in the system Al_2O_3-TiO_2-CaO
All experiments in Pt capsules 0.5-1.0 hrs, 5 kbar.

Exp.	Starting Comp.		Temp. °C	Products	Melted
1.	$CaTi_4Al_{10}O_{24}$	m.o.	1400	CTA, Pvsk, Cor	Yes
2.	"	"	1450	" " "	"
3.	"	n.c.	1350	" " "	"
4.	$CaTi_3Al_8O_{19}$	n.c.	1400	" " "	No
5.	"	"	1500	High-Ca CTA, Pvsk, Cor	Yes
6.	$CaTiO_3 + Al_2O_3$	m.o.	1400	Pvsk, Cor	No
7.	" "	"	1500	" "	"
8.	" "	n.c.	1500	" "	"
9.	$CaTi_4Al_{10}O_{24}$	m.o.	1400	CTA, Pb, Cor (?Pvsk)	Yes
10.	$CaTi_3Al_8O_{19}$	n.	1400	CTA, Pb, Cor	"
11.	"	"	1500	" " "	"
12.	$CaTiO_3$+Al_2TiO_5 (1:1 wt)	n.c.	1300	Ru, mixed Ca-Ti-Al oxides	No
13.	" "	m.o.	1400	Pvsk, Pb	Yes
14.	$CaTi_3Al_8O_{19}$ + TiO_2(1:1 wt)	n.	1400	Pvsk, Pb, Ru	"
15.	$CaTi_3Al_8O_{19}$ + TiO_2(1:1 wt)	n.c.	1500	Cor, Pvsk, Ru	"

m.o. = starting composition produced by intimately mixing anatase, $Al(OH)_3$ and $CaCO_3$.

n.c. = starting composition produced by intimately mixing anatase, $Al(NO_3)_3.xH_2O$ and $CaCO_3$.

n. = starting composition produced by intimately mixing anatase, $Al(NO_3)_3.xH_2O$ and $Ca(NO_3)_2.xH_2O$.

Pb = pseudobrookite Al_2TiO_5

Cor = corundum Al_2O_3

Pvsk = perovskite $CaTiO_3$

Ru = rutile TiO_2

CTA = $CaTi_3Al_8O_{19}$

Table 4. Compatibility between Ba-hollandite ($BaAl_2Ti_6O_{16}$) and $CaTi_3Al_8O_{19}$.

Starting Composition	Temp.°C	Products	Melted
CTA + Holl (1:1 wt) n.c.	1300	Holl, Ru, fine-grained CTA phases.	No
" " " "	1350	Holl, Ru, CTA	Yes
" " " m.o.	1300	Holl, Ru, CTA, Cor	No
CTA + $CaZrTi_2O_7$ m.o. (1:1 wt)	1350	CTA + Zirc	?

m.o. = starting composition produced by intimately mixing anatase, $BaCO_3$ $Al(OH)_3$ and $CaCO_3$.

n.c. = starting composition produced by intimately mixing anatase, $BaCO_3$ $Al(NO_3)_3.xH_2O$ and $CaCO_3$.

n. = starting composition produced by intimately mixing anatase, $Ba(NO_3)_2$ $Al(NO_3)_3.xH_2O$ and $Ca(NO_3)_2.xH_2O$.

Holl = hollandite

Ru = rutile

CTA = $CaTi_3Al_8O_{19}$

Zirc = zirconolite

Cor = corundum

All experiments at 5 kbar, 0.5-1.0 hrs duration, Pt capsules.

Table 5. Magnetoplumbite-type phases produced in SYNROC-C formulations.

	A	B	C	D	E
TiO_2	12.9	15.4	16.9	11.6	18.0
Al_2O_3	72.8	67.6	66.1	72.4	61.5
FeO	8.1	9.6	10.5	8.5	13.8
CaO	5.2	6.4	6.4	6.9	7.4
Sum	98.1	99.0	99.5	99.4	100.7

Structural formulae calculated on the basis of 19 oxygens.

Ti	1.007	1.397	1.529	1.036	1.656
Al	10.247	9.608	9.373	10.137	8.870
Fe	0.809	0.968	1.057	0.844	1.412
Ca	0.665	0.827	0.825	0.878	0.970
Sum	12.80	12.80	12.78	12.90	12.91
Ti+Al+Fe	12.1	12.0	12.0	12.0	11.9

Experimental conditions: 5 kbar, 1200-1300°C, 1 hr, Fe capsules.

Starting composition: A,B and C = SYNROC + waste, plus 2-3% Fe metal.
D = synthetic magnetoplumbite-type phase.
E = 30% TiO_2, 47% Al_2O_3, 10% FeO, 12% CaO (see text).

place further definition on the size of the liquid field. Thus by about 1500°C the liquid field has expanded to engulf CTA, and joins from CTA to perovskite, corundum and pseudobrookite disappear, as shown in Figure 2d. (For clarity, the stability field of the incongruent melting product of CTA has not been included). Ultimately the liquid field will expand to eliminate pseudobrookite, hibonite, perovskite and rutile.

The phase relations of pure hibonite ($CaAl_{19}O_{19}$) were not explored in this experimental study. The role of Fe,Ti-bearing magnetoplumbite-type phases in SYNROC formulations is discussed in Section 7 of this paper.

6. Compatibility between CTA and SYNROC minerals

The common occurrence of CTA in many SYNROC-C formulations strongly suggests it is compatible with zirconolite, perovskite and hollandite. The experiments listed in Table 3 establish the coexistence of CTA and perovskite, whilst data in Table 4 confirm that CTA is compatible with hollandite and zirconolite. Its appearance in SYNROC assemblages is generally a result of Al_2O_3 activity being higher than normal. This can occur in various ways, for example, entry of Ti^{3+} into hollandite "releases" Al_2O_3, which in turn reacts with CaO and TiO_2 in zirconolite and perovskite to produce CTA. CTA has also been produced in SYNROC formulations when the quantity of "excess Al_2O_3" incorporated with the inert additives was greater than that currently recommended (~1%).

7. Characterization of Magnetoplumbite-type phases

Iron-bearing Ca-Ti-Al phases possessing the magnetoplumbite structure have been synthesised in various SYNROC formulations where metallic iron (or cobalt) had been introduced in order to control redox state. Typical examples are given in Cols. A, B, and C of Table 5. Col. D contains the microprobe analysis of one such magnetoplumbite-type phase synthesised separately for X-ray characterization.

An unusual Ca-rich example would contain 30% TiO_2, 47% Al_2O_3, 10% FeO and 12% CaO. It is probably metastable because subsequent attempts to synthesise it alone for further characterization were unsuccessful. The product assemblage instead contained a magnetoplumbite-type phase (Col. 6, Table 5) plus perovskite and Fe-bearing pseudobrookite.

8. Crystal chemistry of magnetoplumbite-type phases

The mineral magnetoplumbite ($PbFe_{12}O_{19}$) is the type-example of a particular crystal structure $XY_{12}O_{19}$ related to β-Al_2O_3. The latter structure is a fast ionic conductor in which large cations e.g. sodium can move freely along conduction planes between spinel-type blocks. In magnetoplumbite, the inter-spinel layers also have unusual 5-fold coordinated sites which can accommodate smaller cations. Morgan et al. (1981) are exploring the suitability of magnetoplumbite phases as components of a ceramic wasteform. They have shown that the "X" cation site may be occupied by Na,Cs, Ca, Sr, Ba, $Na_{0.5}$, $REE_{0.5}$. Small cations may substitute into the Al,Fe spinel blocks if required for charge-balance. For example Ba^{2+} and Al^{3+} in $BaAl_{12}O_{19}$ can be replaced by La^{3+} and Mg^{2+} to give a new magnetoplumbite-type phase, $LaMgAl_{11}O_{19}$.

Keil and Fuchs (1971) have studied the mineral hibonite, a calcium-aluminate magnetoplumbite-type phase which occurs naturally in meteorites, and have found that Cr, Ti and Mg may enter the structure. We have successfully synthesised a magnetoplumbite-type phase with half its Ca^{2+} replaced by Sr^{2+}. However, in SYNROC assemblages, perovskite and not the magnetoplumbite-type phase remains the major host for strontium. Our exploratory studies of a high-alumina SYNROC-D wasteform (Kesson and Ringwood, 1981) revealed that Mn and Na could also be accommodated, but there is as yet no independent evidence to confirm the belief of Morgan et al. (1981) that both Cs and Si can simultaneously enter the magnetoplumbite structure.

The analyses of magnetoplumbite-type phases in Table 5 are characterised by deficient cation sums for a structure based on 19 oxygen atoms. The structural formulae reveal that the deficiency is related to vacancies in large-cation ("X") sites, whilst the "Y" sites, occupied by Al, Ti and Fe, remain essentially full. Interestingly, near-integral cation sums ($\sim$2) are obtained in most cases for structural formulae based on 3 oxygens. The significance of this is not understood.

9. Compatibility relations of magnetoplumbite-type phases in SYNROC-C

Magnetoplumbite-type phases coexists with hollandite, perovskite, zirconolite and Fe-bearing pseudobrookite. They do not

coexist with the CTA phase $CaTi_3Al_8O_{19}$. (In the simple system Al_2O_3-TiO_2-CaO the corundum-perovskite join prohibits CTA from coexisting with hibonite $CaAl_{12}O_{19}$, a magnetoplumbite-type structure).

In SYNROC formulations contaminated with iron, magnetoplumbite-type phases may appear together with hollandite, zirconolite and perovskite. Note that the magnetoplumbite-type phases alone is observed, never an Fe-bearing form of the particular CTA phase discussed in Section 2 of this manuscript. Because the manufacture of SYNROC will be carried out under conditions where oxygen fugacities are controlled at low levels, we have not explored the effects of Fe^{3+} in stabilizing CTA versus magnetoplumbite-type phases.

10. Elimination of magnetoplumbite-type phases from SYNROC-C formulations

Magnetoplumbite-type phases are structurally related to the fast ionic conductor β-Al_2O_3, and so we suspect its resistance to groundwater leaching may be far from optimum. It would therefore seem preferable to eliminate it from SYNROC assemblages. Its appearance is related to FeO contamination which occurs when metallic iron is introduced into SYNROC precursors in order to control oxygen fugacities at low levels during hot-pressing. The metallic iron inevitably reduces some Ti^{4+} to Ti^{3+} and is consequently oxidized to FeO. This problem can be eliminated very easily by substituting metallic titanium for metallic iron, as the redox control agent.

11. References

Keil, K. and Fuchs, L. (1971) Hibonite ($Ca_2(Al,Ti_{24})O_{38}$) from the Leoville and Allende chondritic meteorites. Earth Planet. Sci. Lett. 12, 184-190.

Kesson, S.E. and Ringwood, A.E. (1981) Immobilization of highly aluminous sludges. Unpublished report.

Morgan, P.E., Clarke, D.R., Jantzen, C.M. and Harker, A.B. (1981) High alumina tailored nuclear waste ceramics. Jour. Amer. Ceram. Soc., in press.

Oversby, V.M. and Ringwood, A.E. (1981) Leach testing of SYNROC and glass samples at 85°C and 200°C. Nucl. Chem. Waste Management. Submitted for publication.

Immobilization of Highly Aluminous Sludges

S.E. Kesson and A.E. Ringwood

1. Introduction

Two new SYNROC formulations aimed at immobilizing very alumina-rich sludges have been explored experimentally. In the first of these, magnesia (MgO) is included with the other inert SYNROC additives (TiO_2, ZrO_2, SiO_2, CaO, etc.) with the aim of producing a wasteform comprised of zirconolite, perovskite, nepheline and Mg-spinel solid solution. This treatment is analogous to the manufacture of regular SYNROC-D, where iron serves to immobilize alumina as $FeAl_2O_4$ component in spinel. The second alternative involves adding a minimum of inert oxide additives, with the aim of allowing "surplus" alumina in the sludges to recrystallize as corundum during wasteform manufacture.

2. Sludge Composition

The composition of the high-Al sludge is listed in Column 1, Table 1. After calcining under controlled redox conditions, the sludge composition should be approximately that given in Column 2, Table 1. This latter composition was used as the starting point for our experiments. Note that zeolites have been excluded from the waste stream and various oxide species recast to others more appropriate to SYNROC redox conditions, e.g. $U_3O_8 \rightarrow UO_2$, $MnO_2 \rightarrow MnO$ $Fe_2O_3 \rightarrow Fe_3O_4$.

3. SYNROC-D; Mg-formulation

(a) Experimental strategy

In this instance, it is desirable that the final product should consist of zirconolite, perovskite, MgO-bearing spinel ss. and nepheline, and, moreover, there should be a minimum of 10 wt.% each zirconolite and perovskite, in order to allow for "flexibility" in handling potential waste stream variations. The appropriate proportions of inert additives (including MgO) have been calculated accordingly. The results of this exercise are presented in Table 2, which shows that 46.5% of inert additives would be required to immobilize 53.5% calcined sludge. Ideally, the final SYNROC-D

Table 1. High-Al sludge compositions.

	High-Al Sludge		Calcine
SiO_2	0.6	SiO_2	0.6
MnO_2	4.4	UO_2	1.4
U_3O_8	1.3	Al_2O_3	84.8
Al_2O_3	76.1	Fe_3O_4	5.7
Fe_2O_3	5.3	MnO	4.0
CaO	0.4	CaO	0.4
NiO	0.8	NiO	0.9
Na_2O	2.0	Na_2O	2.2
SO_4^{2-}	<0.5	Sum	100.0
zeolite	9.3		
Sum	100.7		

The composition of the calcine (Col. 2) has been derived from the composition of the sludge (Col. 1) in the following manner.

(i) Zeolite has been excluded.
(ii) Certain oxide species have been converted to others more appropriate to hot-pressing redox conditions

$Fe_2O_3 \rightarrow Fe_3O_4$ (enters spinel ss. as Fe^{2+} and Fe^{3+})
$MnO_2 \rightarrow MnO$ (enters spinel ss. as Mn^{2+})
$U_3O_8 \rightarrow UO_2$ (enters zirconolite as U^{4+})

(iii) Sulfate will be lost during calcining.
(iv) Sum recalculated to 100.

wasteform would consist of 6 wt.% nepheline, 12 wt.% each zirconolite and perovskite, and 70 wt.% spinel s.s.

Starting material corresponding to the bulk composition given in the final column of Table 2 was prepared from an intimate well-ground mixture of oxides, hydroxides and carbonates, following our normal laboratory procedures. It was then hot-pressed at 5 kbar and temperatures of 1150°C, 1200°C and 1250°C for 1 hr. Platinum sample capsules were used, so that oxygen fugacity conditions near Ni-NiO would prevail during hot-pressing.

(b) Experimental results

X-ray diffraction studies showed that at 1100°C, perovskite and spinel were well-crystallized. The characteristic zirconolite lines could also be identified. In the higher temperature runs, the intensities of the zirconolite lines increased relative to perovskite and spinel. The characteristic lines of nepheline could not be confirmed in any run, however, with only ~6% nepheline in the assemblage this is not entirely unexpected. Relict TiO_2 was also identified in the 1100°C run. In polished section, the 1100°C and 1200°C runs were very fine-grained, whilst the poor polish on the 1100°C strongly suggested incomplete reaction. This was subsequently confirmed by microprobe examination, which revealed traces of relict TiO_2 and ZrO_2. The 1250°C run consisted of a homogeneous equigranular material, with grain size 1-10μ, with spinel typically forming the larger grains. Representative microprobe analyses of zirconolite and spinel are presented in Table 3. Perovskite was too finely crystalline for successful analysis - and the presence of nepheline was never confirmed with certainty in any run, probably due to its fine grain size and low abundance.

(c) Discussion

In principle, highly aluminous sludges could be immobilized using special SYNROC formulations which include MgO amongst the inert additives. The product wasteform would consist of zirconolite, perovskite, nepheline and spinel ss., with the MgO serving to immobilize the bulk of the alumina as $MgAl_2O_4$ component in spinel solid solution. One advantage of this process would be the comparative ease with which redox conditions could be controlled. However, there are some potential problems with the strategy.

Table 2. SYNROC-D; Mg-formulation.

	53.5% SLUDGE CALCINE	46.5% INERT ADDITIVES	BULK SYNROC
SiO_2	0.3	2.0	2.3
TiO_2	-	15.2	15.2
ZrO_2	-	3.9	3.9
UO_2	0.8	-	0.8
Al_2O_3	45.4	-	45.4
Fe_3O_4	3.1	-	3.1
MgO	-	18.8	18.8
MnO	2.1	-	2.1
NiO	0.5	-	0.5
CaO	0.2	6.3	6.8
Na_2O	1.2	-	1.2
Sum	53.6	46.5	100.1

Ideal Mineralogy (wt.%) Nepheline 6
Zirconolite...12
Perovskite....12
Spinel s.s....70

Table 3. Analyses of spinel and zirconolite in Mg-bearing SYNROC-D.

	Spinel ss.	Zirconolite
TiO_2	4.8	42.9
ZrO_2	-	31.8
UO_2	-	5.5
Al_2O_3	62.2	1.1
MgO	26.2	0.7
FeO	3.8	1.3
MnO	2.8	0.9
NiO	0.3	-
CaO	0.3	14.4
Sum	100.4	98.6

Perovskite and nepheline too fine-grained for analysis.

Firstly, it appears that equilibrium is achieved only over a narrow temperature interval near the solidus. Moreover, the temperatures involved are quite high (around 1200°C) and careful control of hot-pressing conditions would be critical. Other problems would arise if the proposal to incorporate fragmented Cs-bearing hollandite into SYNROC-D were followed. At 1200°C, the hollandite melts and reacts vigorously with the SYNROC matrix, and no longer serves to immobilize cesium.

4. SYNROC-D : Corundum formulation

(a) Experimental strategy

In this formulation, the aim is to incorporate the minimum amount of inert additives to yield a product assemblage consisting of zirconolite and perovskite (a minimum of 10 wt.% of each) plus nepheline, spinel ss. and corundum. The mineralogy of the product wasteform would differ significantly from other SYNROC-D formulations in that the modal proportion of spinel would be relatively small. The spinel phase is produced by the combination of iron, manganese and nickel in the sludges with some alumina. The "excess" alumina remaining should crystallize as abundant corundum. The product assemblage might also contain other aluminous phases, such as a magnetoplumbite-type phase ($XY_{12}O_{19}$), the CTA phase $CaTi_3Al_8O_{19}$, or pseudobrookite. (This latter phase would necessarily be fairly Fe-rich, in order to coexist with perovskite since pure Al_2TiO_5 and perovskite are incompatible). The experimental strategy was aimed at determining whether the above strategy were viable, and at confirming the mineralogy of the product assemblage.

The proportions of inert additives (Table 4) were calculated according to the requirements that all sodium in the sludges be converted to nepheline, and that there should be about 10 wt.% each of perovskite and zirconolite in the final product. The resultant waste-loading is 74%.

Starting material corresponding to the bulk composition in Column 3, Table 4 was prepared from mixed oxides, hydroxides and carbonates according to our preferred procedures. Hot-pressing was carried out for 1 hr. at temperatures of 1200°C in Ni and Pt capsules, and at 1250°C and 1300°C in Ni capsules. The products were examined by X-ray diffraction and electron microprobe analysis.

Table 4. SYNROC-D : Corundum formulation.

	74% SLUDGE CALCINE	26% INERT ADDITIVES	BULK SYNROC
SiO_2	0.4	2.7	3.1
TiO_2	-	12.9	12.9
ZrO_2	-	4.0	4.0
UO_2	1.0	-	1.0
Al_2O_3	62.7	-	62.7
Fe_3O_4	4.2	-	4.2
MnO	3.0	-	3.0
NiO	0.7	-	0.7
CaO	0.3	6.4	6.7
Na_2O	1.6	-	1.6
Sum	73.9	26.0	99.9

Ideal mineralogy (wt.%)

Nepheline	7
Zirconolite	9
Perovskite	12
Spinel ss.	∿15
Corundum	∿57

Table 5. Magnetoplumbite-type phases crystallized from SYNROC-D (Corundum formulation).

	A	B	C	D	E
TiO_2	10.1	11.4	10.5	10.3	14.1
Al_2O_3	73.3	72.2	72.7	73.8	68.1
FeO	3.5	4.1	3.4	4.1	3.7
NiO	0.8	0.2	2.4	0.0	1.4
MnO	3.4	3.6	3.2	3.1	3.4
CaO	6.8	6.6	6.5	6.8	7.9
Na_2O	1.3	1.0	1.2	1.5	0.8
Sum	99.2	99.1	99.9	99.6	99.4

Structural formulae based on 19 oxygens

Ti	0.903	1.021	0.938	0.916	1.276
Al	10.274	10.139	10.179	10.280	9.655
Fe	0.348	0.409	0.338	0.405	0.372
Ni	0.343	0.019	0.229	0.0	0.136
Mn	0.077	0.363	0.322	0.310	0.346
Ca	0.866	0.843	0.827	0.861	1.018
Na	0.300	0.231	0.276	0.344	0.187
Sum	13.11	13.02	13.11	13.12	12.99

Starting composition: "Bulk SYNROC" as in Table 4.

Experimental conditions: 5 kbar, 1 hr, A at 1200°C Ni capsule
B " 1200°C Pt "
C " 1250°C Ni "
D " 1100°C Ni "
E " 1300°C Ni "

(b) Experimental results

The product assemblages consisted of abundant needles (~20 μ) of a magnetoplumbite-type phase in a fine-grained matrix. Neither spinel, nepheline, corundum nor perovskite were identified by microprobe or X-ray, although minor zirconolite and baddelyite were observed. Analysis of the magnetoplumbite-type phases (Table 5) revealed that they were similar to hibonite ($CaAl_{12}O_{19}$) with minor substitution of Na for Ca and Mn,Ti,Ni and Fe for Al.

The fine grain size of the matrix in the above experiments did not permit microprobe analysis of phases coexisting with the magnetoplumbite. A second series of experiments on a moderately aluminous sludge composition carried out just above the solidus temperature established that perovskite, zirconolite, spinel, a Cs-rich "nepheline" and Cs-free nepheline could coexist with the magnetoplumbite-type phase. An example of this compatible phase assemblage is presented in Table 6.

(c) Discussion

The various experiments described above demonstrate that it is not possible to convert highly-aluminous sludges to a wasteform comprising zirconolite, perovskite, spinel and nepheline plus corundum, by adding appropriate minimum amounts of the inert SYNROC additives (CaO, TiO_2, ZrO_2, SiO_2). The product mineralogy is instead dominated by a calcium-aluminate phase with the magnetoplumbite structure. This phase was found to accommodate minor amounts of Ti, Mn, Ni, Fe and Na in solid solution.

Scientists working for Rockwell International have advocated that highly-aluminous sludges be converted to a wasteform whose mineralogy is dominated by a magnetoplumbite-type phase (e.g. Morgan et al., 1981; Harker et al., 1981). A very similar product has been obtained in the above series of experiments as a direct result of following the SYNROC strategy first described by Ringwood (1978) and subsequently modified for defense waste immobilization (Ringwood et al., 1980).

5. Conclusion

Geological data lead us to suspect that a wasteform dominated by the inert and refractory phase corundum would have been superior to one containing a magnetoplumbite-type phase, in terms of its resistance to groundwater leaching. For this reason we do

Table 6. Magnetoplumbite-type phase plus coexisting phases in moderately-aluminous SYNROC-D formulation.

	Bulk	Zirc	Pvsk	Sp	Cs-neph	Mtpb
SiO_2	6.8	-	-	-	33.7	-
TiO_2	17.5	34.6	53.6	3.9	-	15.1
ZrO_2	5.5	33.6	0.3	-	-	-
UO_2	2.0	10.5	3.9	-	-	-
Al_2O_3	20.1	1.8	1.3	49.5	28.3	61.2
REE*	3.	<.5	1.5	-	-	-
FeO	22.8	4.8	2.3	36.1	0.5	14.5
MnO	5.3	1.7	0.7	9.3	0.3	2.7
NiO	2.5	-	tr.	1.0	-	1.4
CaO	7.1	11.3	34.1	-	0.4	4.8
Na_2O	4.0	0.3	0.2	-	11.6	-
Cs_2O	0.3	SrO=1.1	SrO=1.0	-	26.0	-
Sum	100.4	99.7	98.9	99.8	100.8	99.7

Also present: Glass of variable composition; nepheline, essentially $NaAlSiO_4$.

"BULK" = zirconolite
Pvsk = perovskite
Sp = spinel ss.
Cs-neph = Cs-rich nepheline
Mtpb = magnetoplumbite-type phase

Experimental conditions: 5 kbar, 1200°C, Ni capsule, 1 hr.

*REE = Ce_2O_3 + Nd_2O_3

not advocate converting highly-aluminous sludges to the latter mineralogy. The strategy described earlier in this paper, whereby the "excess" alumina was immobilized as $MgAl_2O_4$ spinel requires comparatively high temperature in order to achieve an equilibrium product assemblage. However, our preferred approach would be to incorporate FeO rather than MgO, which would similarly serve to immobilize alumina as $FeAl_2O_4$ spinel component but at lower hot-pressing temperatures. This latter option could be readily carried out by mixing high-iron sludges with high-alumina sludges, and eliminating the handling of high-alumina sludges as a separate waste-stream.

6. References

Harker, A.B., Jantzen, C.M., Morgan, P.E. and Clarke, D.E. (1981) Tailored ceramic nuclear waste forms: preparation and characterization (Abstract). Amer. Ceram. Soc. Ann. Mtg.

Morgan, P.E., Clarke, D.R., Jantzen, C.M. and Harker, A.B. (1981) High alumina tailored nuclear waste ceramics. Jour. Amer. Ceramic Soc., in press.

Ringwood, A.E. (1978) "Safe disposal of high-level nuclear reactor wastes: A new strategy". Aust. Natl. Univ. Press, Canberra, 64p.

Ringwood, A.E., Kesson, S.E. and Ware, N.G. (1980) Immobilization of US defense wastes using the SYNROC process. In "Scientific Basis for Nuclear Waste Management, vol. 2", 265-272, Ed. G. McCarthy, Plenum Press, N.Y.

SYNROC-D FORMULATIONS PRODUCED BY SINTERING IN AIR

INTRODUCTION

SYNROC-D formulations adapted for the immobilization of the average Savannah River composite sludge (Table 1) have previously been prepared according to recommended procedures, by hot-pressing under controlled redox conditions (reducing) so that a large proportion of iron is present in the divalent state. In this report we investigate the possiblity of preparing SYNROC-D under oxidising conditions by the simpler procedure of sintering in air, at temperatures appreciably above the solidus (1200-1250°C). A dense (95%) material with low porosity can be produced in this manner. Its mineralogy and phase chemistry have been investigated, and the partition behaviour of key radwaste elements such as strontium and uranium has been established.

EXPERIMENTAL PROCEDURES

Pelletized fragments of SYNROC-D were suspended in Pt containers in vertical furnaces for periods of 1-5 hours. The products were examined by X-ray diffraction and electron microprobe.

PHASE CHEMISTRY OF SYNROC-D AFTER SINTERING IN AIR

The SYNROC-D material produced by sintering in air at 1200-1250°C does not possess the typical phase assemblage (zirconolite, perovskite, spinel and nepheline). Instead, one or more new oxide phases plus a low-silica glass are observed and primary nepheline was not positively identified.

The accompanying Tables 2 and 3 present analyses of coexisting phases produced in two sintering runs at 1200°C. The 1½ hour run (Table 2) yielded a phase assemblage of fine-grained perovskite, rare ilmenite, intergranular films of glass, a hibonite-type phase of variable composition and two chemically-distinct zirconolites, differing mainly in their UO_2 and ZrO_2 contents. A longer run of 5 hours duration (Table 3) yielded fine-grained perovskite, zirconolite, a hibonite-type phase, and nepheline. The unusually high TiO_2, Fe_2O_3 and CaO

TABLE 1

SYNROC-D FORMULATION DESIGNED TO IMMOBILIZE

AVERAGE SAVANNAH RIVER SLUDGE

SiO_2	7.4
TiO_2	18.8
ZrO_2	5.6
UO_2	2.2
Al_2O_3	19.8
Ce_2O_3	0.6
Nd_2O_3	0.6
Fe_2O_3	25.3
MnO	5.1
NiO	3.3
CaO	7.3
SrO	0.3*
Na_2O	3.5
Cs_2O	0.3
SUM	100.1

This composition was used in the SYNROC-D sintering experiments as described in this report.

* An additional 1% SrO was subsequently added for partition experiments.

TABLE 2

PHASES PRODUCED IN SYNROC-D AFTER SINTERING IN AIR FOR 1½ HOURS AT 1200°C.

	Zirconolite (a)	Zirconolite (b)	Hibonite-type phase variable composition			Ilmenite
TiO_2	31.7	26.3	17.9	→	12.7	38.5
ZrO_2	32.7	43.9	--		--	--
UO_2	10.7	5.0	--		--	--
CeO_2	2.6	1.5	--		--	--
Al_2O_3	1.4	2.4	30.7		43.0	7.6
Fe_2O_3	7.0	8.7	34.0		28.4	19.4
FeO	--	--	--		--	29.8
NiO	0.3	0.8	3.9		3.1	0.5
MnO	1.4	2.0	7.0		6.0	3.9
CaO	11.9	10.2	6.3		5.1	0.2
SrO	<.2	<.2	--		--	--
Na_2O	<.2	<.2	1.5		1.5	--
SUM	99.7	100.5	101.2		99.8	99.9

Perovskite too fine-grained for satisfactory analysis.

Glassy Na,Si-rich material at grain boundaries.

Experimental Conditions: "SC" composition sintered in air at 1200 C, 1½ hours.

All iron expressed as Fe_2O_3 in zirconolite and hibonite.

TABLE 3

PHASES PRODUCED IN SYNROC-D AFTER SINTERING IN AIR FOR 5 HOURS AT 1200°C

	Zirconolite	Hibonite-type phase	(Quench) Nepheline
SiO_2	--	--	41.5
TiO_2	32.1	16.7	0.5
ZrO_2	32.0	--	--
UO_2	10.5	--	--
REE*	2.5	--	--
Al_2O_3	1.6	26.7	35.8
Fe_2O_3	8.6	38.0	1.7
FeO	--	--	--
NiO	0.2	4.6	--
MnO	1.4	7.5	0.1
CaO	12.1	4.6	3.3
SrO	0.6	0.8	--
Na_2O	<.2	1.7	17.2
SUM	101.4	100.6	100.3

Perovskite is present but way too fine-grained for satisfactory analysis; however, it contained both Nd_2O_3 and SrO (∿4%), and UO_2 (∿0.5%).

Glass also present at grain boundaries.

Experimental conditions: "SC" composition sintered in air at 1200°C for 5 hours.

All iron expressed as Fe_2O_3.

* REE = CeO_2 + Nd_2O_3

contents of the nepheline are consistent with its formation during quenching. Intergranular glassy material is also present but could not be analysed successfuly. A better approach to an equilibrium assemblage was probably obtained in this 5 hour run, as evidenced by the narrow composition range for both zirconolite and the hibonite-type phase, and the absence of ilmenite.

Positive confirmation of the identity of the hibonite-type phase which appears in the above experiments was achieved by means of a separate series of synthesis experiments on a bulk composition similar to that in col. 2, Table 3, whereby pelletized fragments were heated in air at 1200, 1250 and 1300°C for 1-2 hours. At 1200°C reaction was incomplete. At 1250°C and 1300°C the products consisted largely of a hibonite-type phase (col. 1, Table 4) plus trace amounts of another uncharacterized Ca-Ti-Al-Fe phase. The crystal structure of the hibonite-type phase was confirmed from its X-ray diffraction pattern. (Hibonite, $CaAl_{12}O_{19}$, is isostructural with magneto-plumbite ($PbFe_{12}O_{19}$). The structural formula indicates some solid solution towards β-Al_2O_3 ($NaAl_{11}O_{17}$) because the cation sum (Ca + Na) is slightly in excess of unity. Ti^{4+} must enter the structure via a coupled substitution whereby $Ti^{4+} + M^{2+}$ exchange for two trivalent ions (Fe^{3+} and Al^{3+}). There is insufficient Mn^{2+} and Ni^{2+} to balance all the Ti^{4+} hence some of the iron must also be present in the divalent state, although this would amount to less than 15% of the total amount of iron in the phase. It follows that most of the iron is present in the +3 state, as might be expected from the highly oxidising synthesis conditions.

It is evident that whilst some SrO enters both hibonite and zirconolite, perovskite remains the major host for Sr. Substantial amounts of UO_2 are taken up by zirconolite, however some uranium, presumably in the hexavalent state, may occur in the glass. More specific evidence for this was obtained in runs at 1225°C and 1250°C where the glasses commonly contained from 1 to 5% of UO_2. Rare earths are partitioned into zirconolite and perovskite and were not detected in glass or hibonite. Most Cs_2O is lost during the heat-treatment, however any residual Cs would be expected to partition into the glass.

TABLE 4

SYNTHESIS OF HIBONITE-TYPE PHASE

	Hibonite-type phase	Rare uncharacterised Ca-Ti-Al-Fe phase
TiO_2	14.8	28.2
Al_2O_3	34.1	20.5
Fe_2O_3	36.2	25.3
MnO	5.7	4.7
NiO	3.2	3.1
CaO	4.6	16.7
Na_2O	1.5	1.1
SUM	100.1	99.6

Structural formula based on 19 oxygens. Fe''' amd Fe'' calculated assuming atomic (Mn +Ni + Fe'')= Ti

Ti	1.541	
Al	5.566	
Fe'''	3.257	
Fe''	0.516	
Mn	0.669	1.025
Ni	0.356	
Ca	0.683	1.083
Na	0.403	
SUM	12.991	

Experimental conditions:sintered in air at 1300°C for 1 hour.

Sintering SYNROC-D in air at 1225°C for 3 hours resulted in a different phase assemblage in which zirconolite was destabilized in favour of a new face-centred cubic (defect-fluorite-type) structure. The product phase assemblage is shown in Table 5.

The identity of the new defect fluorite-type phase was confirmed in separate synthesis experiments involving sintering in air at 1250, 1300 and 1350°C for 0.5 and 2 hours. The products at all temperatures consisted of a two-phase assemblage, predominantly the defect-fluorite-type phase, plus minor zirconolite. An example of the coexisting pair is provided in Table 6. It is difficult to deduce much about the crystal chemistry of this new phase, except to note that a large proportion of its iron is probably in the ferrous state, because a good value for the oxide sum (99.5%) is obtained with all iron expressed as FeO.

The partition behaviour of strontium differs from that observed at 1200°C, with larger amounts entering the hibonite-type phase compared to perovskite, and some also partitioning into the new defect-fluorite-type phases. Zirconolite, as noted earlier, is no longer stable, and so perovskite serves as the main host for rare earths. Although some UO_2 is contained in the defect-fluorite-type phases, a significant amount can be found in the interstitial glass, where it presumably occurs in the hexavalent state. The leaching performance of a wasteform with so much of its uranium in glass rather than in crystal lattice sites, is likely to be rather poor.

After sintering in air for 1.5 hours at 1250°C further modification of the phase assemblage was observed. The product consisted of small perovskite grains, together with abundant hibonite-type and defect-fluorite-type phases, the latter showing a range of composition. Zirconolite was again absent, however a ferric spinel was observed. (This is the first occurrence of spinel in this particular experimental study.) Interstitial glass was also present. Analyses of coexisting phases are presented in Table 7.

TABLE 5

PHASES PRODUCED IN SYNROC-D AFTER SINTERING IN AIR FOR 3 HOURS AT 1225°C

	Hibonite-type phase	Defect-fluorite-type phases (a)	(b)	Glass
SiO_2	--	--	--	31.5
TiO_2	16.0	32.2.	31.2	13.7
ZrO_2	--	22.8	13.9	0.9
UO_2	--	5.2	1.0	4.8
REE	--	--	1.0	--
Al_2O_3	26.2	5.7	9.9	21.9
Fe_2O_3	38.8	--	--	--
FeO	--	16.6	25.0	6.5
MnO	7.1	3.7	5.4	2.2
NiO	4.6	0.5	1.2	0.1
CaO	4.6	10.5	9.9	11.2
SrO	3.0	0.3	1.0	--
Na_2O	1.2	0.3	0.7	6.4
SUM	101.3	99.6	100.2	99.2

Fine-grained Perovskite contains 1.2% SrO, 0.2% UO_2 and ~5% rare earths.

All iron expressed as Fe_2O_3 in hibonite, otherwise all as FeO.

TABLE 6

COEXISTING DEFECT-FLUORITE-TYPE PHASE AND ZIRCONOLITE

	DEFECT-FLUORITE-TYPE PHASE	ZIRCONOLITE
TiO_2	31.8	31.5
ZrO_2	14.3	34.2
UO_2	1.8	6.5
REE	∿1.0	∿3.0
Al_2O_3	10.7	1.5
FeO	22.7	8.7
MnO	5.0	1.4
NiO	1.8	0.4
CaO	9.3	11.8
SrO	0.4	0.9
Na_2O	0.7	0.3
SUM	99.5	100.2

Experimental conditions: Pellet sintered in air at 1350°C for 0.5 hours.

TABLE 7

COEXISTING PHASES PRODUCED IN SYNROC-D AFTER SINTERING IN AIR FOR 1½ HOURS AT 1250°C.

	Hibonite-type phase	Defect-fluorite-type phase (variable composition)			Spinel	Glass
SiO_2	--	--	→	--	--	34.2
TiO_2	15.1	31.7		29.7	2.5	4.0
ZiO_2	--	26.6		14.4	--	0.2
UO_2	--	7.4		2.2	--	3.4
REE	--	∿1.		∿2.	--	<.2
Al_2O_3	32.3	4.1		9.7	14.0	29.0
Fe_2O_3	37.2	--		--	47.6	6.6
FeO	--	11.6		23.3	3.9	--
MnO	5.3	2.4		5.2	15.6	1.9
NiO	4.3	1.5		2.8	16.3	1.2
CaO	4.8	10.6		8.5	0.2	4.6
SrO	0.4	0.3		0.4	--	--
Na_2O	1.5	0.3		0.4	--	12.6
SUM	100.9	97.5		98.9	99.9	97.7

Fine-grained perovskite also present.

Experimental conditions: Sintered in air at 1250°C for 1.5 hours.

Because perovskite is too small for satisfactory microprobe analysis it is not possible to confirm the partition behaviour of strontium, although mass-balance consideration suggest that perovskite remains the primary strontium host. Some uranium is contained in the defect-fluorite-type phase, however, significant amounts are also present in the glass, presumably in the hexavalent state, and potentially readily leached. Most of the iron in the spinel and hibonite-type phases is in the oxidised state, whereas the defect-fluorite-type phase appears to contain both ferric and ferrous iron.

CONCLUSIONS

Sintering of SYNROC-D in air at temperatures just above the solidus (1200-1250°C) produces a dense compact ceramic, however the optimum SYNROC-D mineralogy is not produced. Although perovskite is present throughout, spinel appears only at 1250°C, whilst zirconolite is destabilized in favour of a defect-fluorite-type phase above 1200°C. A new, highly oxidised phase structurally similar to hibonite is common throughout and may contain significant amounts of strontium and sodium. Nepheline was identified only as a byproduct of quenching. The interstitial liquid contains substantial amounts of uranium which may well be readily leachable. Moreover, any neptunium present in the waste would probably be converted to a highly oxidised species which would preferentially partition into the glassy phase. Most cesium is lost by volatilization. A SYNROC-D wasteform produced by sintering in air is not expected to display good leaching behaviour for U, Np and other actinides. For this reason, production of SYNROC-D by air - sintering is not recommended.

The wide field of stability of the hibonite-type phase is interesting. It co-exists with zirconolite, perovskite, spinel and probably with nepheline. It has previously been encountered when hot-pressing SYNROC-D in platinum capsules under moderately oxidising conditions (early report by A.E. Ringwood to J. Tewhey) but its crystal structure was not identified.

The hibonite phase (ideally $CaAl_{12}O_{19}$) present in these runs contains a large amount of divalent elements e.g. Mn^{2+}, Ni^{2+}, some Fe^{2+}, (as well as much Fe^{3+}) and charge balance is achieved by entry of an equivalent amount of Ti^{4+} ($M^{2+}+Ti^{4+}=2Al^{3+}$). This phase is also capable of accepting a substantial amount of sodium although surprisingly, the complex substitution of (Na^{+} + REE^{3+}) for 2 Ca^{2+} reported by Rockwell, was not observed. The hibonite produced in the present series of runs contained a large amount of Fe^{3+}. It is conceivable that hibonite could be a stable phase in SYNROC-D formulations prepared under more reducing conditions if there were sufficient Ti^{4+} to charge-compensate for Fe^{2+} (Ti^{4+} + Fe^{2+} = $2Al^{3+}$). This possibility should be investigated since hibonite could be a suitable host for sodium if the sodium content of the sludges could be reduced by more intensive washing. However, there are certain properties of hibonite which require additional study before it can be seriously considered as a component of SYNROC-D. These include the resistance to leaching of hibonites containing substantial amounts of sodium and the effects of radiation damage on this phase.

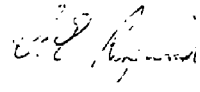

Crystallization behaviour of interstitial glass in SYNROC-D formulations

1. INTRODUCTION

A new estimate of the composition of the average Savannah River sludge has recently become available. This report summarizes an experimental study of the incorporation of the new average sludge composition into SYNROC-D formulations and the crystallization behaviour of liquids in those systems. In some hot-pressing experiments carried out at 1100°C, a significant amount of interstitial glass was observed in addition to the major phases spinel ss., perovskite, zirconolite and nepheline. The presence of glass in SYNROC-D is undesirable, since it might serve as a host for cesium and strontium, and could lead to unacceptably high leach-rates for these elements. Accordingly, a further series of experiments was carried out in order to characterize the glass and to specify a process for its elimination. The recommended procedures are discussed in this report.

2. EXPERIMENTAL METHODS

Starting materials were prepared from oxide-hydroxide-carbonate mixtures following standard procedures as used in this laboratory. A total of 32 hot-pressing runs were carried out in a piston-and-cylinder apparatus at pressures of 5 kbar, and temperatures ranging from 1200° to 900°C, over periods of 1-3 hours. The products were examined by X-ray diffraction, microscopic and microprobe techniques. Compositions of starting materials

were checked by microprobe bulk analysis of samples hot-pressed at subsolidus conditions (~900°C).

3. INCORPORATION OF AVERAGE SAVANNAH RIVER SLUDGE INTO SYNROC-D

Table 1, column 1, presents the bulk composition of the new average sludge(after calcination), together with appropriate proportions of SYNROC additives (CaO, SiO_2, TiO_2, ZrO_2). This material was hot-pressed at 1100° and 1200°C in Ni capsules to produce the desired SYNROC mineralogy. The composition was further modified by the addition of more SiO_2 such that the molar ratio of SiO_2:Na_2O was increased from an initial value o 2:1, to 2.5:1, 3:1 and 4:1. These three modified compositions were also hot-pressed in Ni at 1100° and 1200°C. The objectiv· of these latter experiments was to study the effects of SiO_2 activity upon the stability of SYNROC-D minerals, and on the composition of the glasses.

At 1100°, all four starting compositions (molar SiO_2:Na_2O = 2:1, 2.5:1, 3:1 and 4:1 respectively) yield d assemblages consisting of magnetite-rich spinel, fine-grained perovskite and zirconolite, interstitial Al-rich glassy materials, and rare relicts of unreacted ZrO_2 and Al_2O_3. Nepheline was not identified by microprobe, but was confirmed by X-ray diffraction.

In order to obtain a better approach to equilibrium a second series of hot-pressing runs was carried out at 1200°C. All compositions were found to contain large crystals of perovskite and aluminous spinel, and small crystals of nepheline. Zirconolite was too small for quantitative analysis, its presence being confirmed by X-ray diffraction. Analyses of coexisting phases are presented in Table 2. Textural features suggest the composition of the interstitial liquid has been modified by quenching, hence

Table 1. Bulk compositions of starting materials.

	"SC"	"High-neph SC"	"SYN-D Glass 1"	"SYN-D Glass 2"
SiO_2	7.8	23.3	22.9	33.8
TiO_2	18.8	15.3	11.3	8.6
ZrO_2	5.6	5.0	0.3	1.4
UO_2	2.2	1.9	-	-
Al_2O_3	19.8	22.8	29.0	25.4
Ce_2O_3	0.6	0.6[2]	-	-
Nd_2O_3	0.6	-	-	-
Fe_2O_3[1]	25.3	9.5	17.2	9.8
MnO	5.1	2.0	3.4	2.0
NiO	3.3	0.9	1.7	-
CaO	7.3	7.1	5.3	4.6
SrO	0.3	0.3	-[3]	1.0
Na_2O	3.5	12.0	8.7	1
Cs_2O	0.3	1.0	1.0	1.0
Sum	100.0	101.0	100.0	101.0

[1] all Fe as Fe_2O_3.

[2] Sm_2O_3 = 0.6%.

[3] 2% SrO subsequently added for partition experiments.

"SC" New average Savannah River sludge plus SYNROC additives.

"High-neph. S.C." Bulk composition of model SYNROC-D with 55 wt.% nepheline, 15 wt.% each perovskite, zirconolite and spinel.

"SYN-D Glass 1" Interstitial glass in "SC" composition at 1200°C.

"SYN-D Glass 2" Interstitial glass in "High-neph. S.C." at 1200°C.

Table 2. Coexisting phases in "SC", a SYNROC-D formulation designed to immobilize average Savannah River sludge.

	Spinel	Perovskite	Nepheline	Glass
SiO_2	-	-	41.8	35.5
TiO_2	7.1	53.3	-	9.4
ZrO_2	-	<.1	-	0.3
UO_2	-	2.1	-	<.1
Al_2O_3	29.9	-	37.1	23.7
Fe_2O_3	20.0	-	-	-
REE	-	∿4	-	-
FeO	26.4	1.9	-	12.1
NiO	7.5	<.1	-	0.5
MnO	8.7	1.1	-	1.8
CaO	0.3	34.8	-	6.1
SrO	-	1.4	-	<.2
Na_2O	-	1.2	21.0	9.8
Cs_2O	-	-	<.2	<.2
Sum	99.8	99.8	99.9	99.2

Zirconolite too fine-grained for analysis.

Starting composition: as shown in Table 1.

Experimental conditions: 5 kbar, 1 hour, Ni capsule, 1200°C.

the analysed glass composition presented in Column 4 of Table 2, is at best an approximation of the liquid composition.

An important observation in these experiments is that nepheline has crystallized in bulk compositions whose bulk molar SiO_2:Na_2O ratios range from the 2:1 value normally prescribed for SYNROC-D through to very high values (4:1). This demonstrates that SYNROC-D wasteforms would be tolerant to fluctuations in the SiO_2:Na_2O ratio of the waste stream. In other words, large excess quantities of silica would not suppress nepheline crystallization. However, at a given temperature, excess quantities of silica cause an increase in the amount of interstitial glass.

It is significant that the glass compositions (Table 3) remain comparatively low in SiO_2 and high in Al_2O_3, even in compositions with high SiO_2:Na_2O ratios. Apparently the liquid composition is buffered by equilibrium with crystalline phases, namely spinel ss, nepheline, perovskite and zirconolite. Glasses with these unusual compositions are likely to display higher leachabilities than, for example, basaltic aluminosilicate glasses with higher SiO_2 contents. The presence of these glasses in SYNROC-D wasteforms will therefore be undesirable, because elements such as cesium and strontium which might partition into the glass could then be easily leached. On the other hand, the compositions of these glasses, namely low SiO_2 and high TiO_2, FeO and Na_2O suggest that they are likely to have low viscosities, and would crystallize readily with further cooling. Accordingly, a new series of experiments was designed to obtain a better estimate of the compositions of SYNROC-D glasses, so that their crystallization behaviour under controlled cooling conditions could be further evaluated.

Table 3. Glasses produced in "SC" compositions with variable molar SiO_2:Na_2O ratios[1].

SiO_2:Na_2O Temp.	3:1 1100°	4:1 1100°	2:1 1200°	3:1 1200°	4:1 1200°
SiO_2	23.0	23.5	22.2	35.5	37.1
TiO_2	11.4	11.6	10.8	9.4	10.7
ZrO_2	0.4	0.2	0.3	0.3	<.1
Al_2O_3	29.4	26.8	23.9	23.7	22.3
FeO[2]	17.8	14.8	13.8	12.1	11.1
NiO	1.6	2.6	0.9	0.5	0.4
MnO	3.7	4.1	2.5	1.8	2.4
CaO	4.3	7.2	4.3	6.1	7.8
Na_2O	7.8	8.1	10.1	9.8	7.5
Cs_2O,SrO	see footnote[3]				
Sum	99.4	98.9	98.8	99.2	99.3

[1] All runs in Ni capsules at 5 kbar.

[2] All iron expressed as FeO

[3] Cesium volatilizes from the glasses under the impact of the electron beam during microprobe analysis. Accurate measurement of Cs_2O was not possible, however, the high sums (~99%) of all glass compositions suggest Cs_2O contents would be ~1%.

Analytical interferences arise in the determination of low levels of SrO in the presence of SiO_2. The SrO contents of the glasses are probably <0.5%.

4. CHARACTERIZATION OF SYNROC-D INTERSTITIAL LIQUIDS

Accurate determination of the composition of the interstitial liquid in SYNROC-D is beset by many difficulties. Firstly, it is evident that the liquid composition is modified during quenching to glass by precipitation of crystallites. Secondly, the small percentage of glass lies along grain boundaries, in narrow bands, and does not segregate into pools large enough for satisfactory microprobe analyses. This second problem at least, can be overcome by a strategy familiar to experimental petrologists, whereby the proportion of glass relative to crystalline phases can be increased. It depends on the fact that the chemical equilibria between liquid and crystalline phases are independent of the proportions of each phase, providing that the compositions of the phases remain fixed. Accordingly, a modified form of SYNROC-D was prepared, in which the amount of interstitial glass should be greater than for the "SC" series of experiments. This modified composition, "High-neph SC" (Column 2, Table 1) corresponds to an assemblage of the typical SYNROC-D minerals, nepheline, zirconolite, perovskite and spinel ss, but in different proportions, namely 55 wt.% nepheline, and 15 wt.% each of the others.

It is evident from Table 3 that the interstitial SYNROC-D liquids contain large amounts of normative nepheline. It follows that in the "High-neph. SC" composition, in which the modal abundance of nepheline has been increased, the quantity of liquid in equilibrium with residual nepheline, spinel ss, zirconolite and perovskite will also be increased. In this manner, larger volumes of glass occur in the run products, and microprobe analysis is facilitated.

The "High-neph. SC" composition has a molar ratio of SiO_2: Na_2O = 2:1. A modification of this was prepared by adding excess

SiO_2 so that SiO_2:Na_2O = 3:1, in order to observe any change in glass composition as a result of higher SiO_2:Na_2O ratios.

These two nepheline-enriched compositions were hot-pressed in Ni capsules at 1100° and 1200°C. Reaction was incomplete at 1100°C because relict ZrO_2 and Al_2O_3 could be identified, together with perovskite, spinel and glass. In the 2:1 composition nepheline and zirconolite could also be identified. At 1200°C the product assemblages of both compositions (2:1 and 3:1) contained spinel, perovskite, zirconolite, nepheline and glass. Typical examples of the phase assemblages are presented in Tables 4 and 5. Although glass was much more abundant than in the "SC" series of experiments, some difficulties were still experienced in obtaining satisfactory microprobe analyses, because in many instances the glasses were peppered with tiny quench crystallites. It should be emphasised again that the glass analyses presented herein are at best an approximation of liquid compositions because of this problem. Table 6 contains analyses of glasses produced at 1100° and 1200°C in these nepheline-rich compositions.

As mentioned above, all glasses coexist with the major SYNROC-D phases (the high Al_2O_3 content of the 1:2 glass at 1100° probably reflects incomplete reaction of Al_2O_3). Certain chemical trends are evident as a function of increasing SiO_2 content, and run temperature, namely higher SiO_2, TiO_2 and CaO and lower Al_2O_3 contents. Although the starting material was doped with uranium and samarium, neither of these elements can be detected in the glass. This key observation suggests that even if an interstitial glass is produced during SYNROC-D manufacture, trivalent and tetravalent actinides and rare earths would nevertheless be contained in the crystal lattices of zirconolite and perovskite, and

Table 4. Coexisting phases plus glass in "High-neph. SC" with SiO_2:Na_2O - 2:1 (Col. 2, Table 1).

	Perovskite	Zirconolite	Spinel	Nepheline	Glass
SiO_2	-	-	-	44.1	33.8
TiO_2	51.7	32.2	11.8	-	8.6
ZrO_2	0.2	40.3	-	-	1.4
UO_2	5.7	4.3	-	-	$\lesssim$0.2
Sm_2O_3	$\sim$4.0	$\sim$1.0	-	-	-
Al_2O_3	1.6	2.2	23.5	34.7	25.4
Fe_2O_3	-	-	18.9	-	-
FeO	1.4	6.6	30.1	-	8.8
NiO	<.1	0.3	8.9	-	0.2
MnO	0.7	1.8	7.1	-	2.0
CaO	32.2	10.8	0.3	-	4.6
Na_2O	1.3	$\sim$0.3	-	18.8	13.7
Cs_2O	-	-	-	1.4	0.2
Sum	100.3*	99.6	100.6	99.0	98.7

*includes 1.5% SrO.

Starting material: "High-neph. SC" (Column 2, Table 1).

Experimental conditions: 5 kbar, 1200°C 1 hr, Ni capsule.

Note: A fine-grained Cs-rich phase may be present, but positive microprobe identification could not be achieved. A pollucite phase ($CsAlSi_2O_6$) has not been positively identified in any of these experiments. It is possible that pollucite is not in equilibrium with the highly SiO_2-undersaturated liquids produced in these experiments.

Table 5. Coexisting phases plus glass in "High-neph. SC", with SiO_2:Na_2O = 3:1.

	Perovskite	Zirconolite	Spinel	Glass*
SiO_2	-	-	-	41.7
TiO_2	52.9	33.6	19.6	10.3
ZrO_2	0.2	41.1	-	1.2
UO_2	4.3	2.4	-	∿0.2
Sm_2O_3	∿2.	∿1.	-	-
Al_2O_3	1.3	1.8	4.6	22.5
Fe_2O_3	-	-	25.3	-
FeO	1.8	8.1	27.4	7.9
NiO	<.1	0.2	15.9	0.2
MnO	0.4	0.3	6.8	1.8
CaO	35.6	10.6	0.3	6.7
Na_2O	1.6	∿0.4	-	6.3
Cs_2O	-	-	-	1.0
Sum	100.1	99.5	100.0	99.6

Nepheline occurs as numerous small inclusions in perovskite and zirconolite, and also in fine-grained intergrowths with spinel in the interstitial glass.

Starting material: "High-neph. SC" as given in Column 2, Table 1 plus additional SiO_2 so that Na_2O"SiO_2 = 1:3.

Experimental conditions: 5 kbar, 1200°, 1 hour, Ni capsule.

*Analysis may not be very meaningful because of beam overlap onto nepheline and spinel.

Table 6. Analyses of glasses produced[1] in "High-neph. SC" compositions with molar SiO_2:Na_2O = 1:2 and 1:3.

SiO_2:Na_2O Temp. C°	1:2 1100°	1:3 1100°	1:2 1200°	1:3 1200°
SiO_2	23.3	34.4	33.8	41.7
TiO_2	1.9	9.4	8.6	10.3
ZrO_2	0.3	2.4	1.4	1.2
Al_2O_3	47.8	26.2	25.4	22.5
FeO[2]	8.2	7.1	8.8	7.9
NiO	2.2	0.9	0.2	0.2
MnO	2.5	1.7	2.0	1.8
CaO	1.4	4.8	4.6	6.7
Na_2O	11.4	11.9	13.7	6.3
Cs_2O,SrO	see footnote[3]			
Sum	99.3	98.8	98.7	99.6

[1]All runs in Ni capsules, 5 kbar, 1 hour.

[2]All iron as FeO.

[3]Some Cs_2O (~1%?) 13 present in the glass, but this volatilizes under the electron beam, making quantitative analysis impossible. SrO is probably ≤0.5%.

would not partition into the glass. Leach-rates for these elements should therefore remain low.

There are analytical difficulties in determining small abundances of SrO in the presence of SiO_2, nevertheless, there appears to be about 0.5% SrO in the glass. In glasses, cesium volatilizes under the electron beam of the probe, making analysis difficult, however, it seems that most of these glasses contain about 1% or more of Cs_2O.

5. CONTROLLED COOLING AND CRYSTALLIZATION OF SYNROC-D GLASSES

Estimates of the composition of interstitial liquids in SYNROC-D have been obtained as described in Sections 3 and 4 and are summarised in Tables 3 and 6. Two such compositions were selected for controlled cooling and crystallization experiments (Cols. 3 and 4, Table 1). These compositions, "SYN-D Glass 1" and "SYN-D Glass 2" correspond to the glasses produced during hot-pressing at 1200°C in, respectively, "SC" composition, and "High-neph. SC, SiO_2:Na_2O = 2:1". The suitability of these two compositions as model interstitial liquids was verified by X-ray diffraction study of both compositions following devitrification at 900°C. In both cases, the SYNROC-D phases spinel ss, perovskite and nepheline were observed. (The low bulk abundance of ZrO_2 in these compositions precludes identification of zirconolite). Furthermore, in subsequent melting experiments these same phases were found to crystallize from both compositions. This evidence of saturation with SYNROC-D phases likewise confirms the suitability of using "SYN-D Glass 1" and "SYN-D Glass 2" compositions as model interstitial liquids.

The "SYN-D Glass 1" composition was cooled linearly from

1100° to 900°C over 2 hours in Fe capsules, and similar cooling runs were conducted from 1200° to 900°C in both Fe and Pt capsules. The product assemblages consisted of nepheline, spinel ss, perovskite, and possible residual glass in the Pt-encapsulated run. Analytical data in Table 7 show that cesium is taken up by nepheline as it precipitates (mass-balance considerations indicate that trace quantities of another Cs-rich phase may also have been precipitated).

The partition behaviour of strontium was studied in a separate experiment. Analytical interferences pose problems for the detection of small amounts of strontium in silicate glass; but these were overcome by doping the starting material (Col. 1, Table 1) with ∿2% SrO and cooling it in Fe capsules from 1200° to 1050°C in order to obtain a product assemblage of nepheline, spinel, perovskite and glass. The perovskite was found to contain 4-5% SrO whilst the glass contained less than 0.5% SrO. The pronounced partitioning of Sr into perovskite is most encouraging. It suggests that most or all of the strontium in interstitial liquids which develop during hot-pressing of SYNROC-D at 1000-1200°C could be incorporated into the relatively leach-resistant perovskite phase by slow-cooling to 800-900°C. Likewise, most of the cesium in the glass could be incorporated into crystalline phases, mainly nepheline.

The other model liquid composition, "SYN-D Glass 2" (Col. 4, Table 1) was similarly cooled from 1200° to 900°C in Fe and Pt capsules. In Fe capsules perovskite, spinel, rare zirconolite and two types of nepheline were identified (Table 8). X-ray diffraction confirmed that nepheline was very abundant. The two types of nepheline differ in that tyep (b) contains more Si, Ti, Fe, Mn, and Cs than type (a) and probably represents a late-

Table 7. Coexisting phases precipitated as a result of slow-cooling of "SYN-D Glass 1".

(A) Assemblage produced in Fe capsule

	Spinel	Perovskite	Nepheline
SiO_2	-	-	40.1
TiO_2	26.2	57.2	0.8
Al_2O_3	12.3	0.4	36.6
Fe_2O_3	4.2	-	-
FeO	49.4	1.3	1.0
NiO	<.1	<.1	-
MnO	8.1	0.9	0.2
CaO	0.1	39.8	0.7
Na_2O	-	0.5	17.3
Cs_2O	-	-	2.6
Sum	100.3	100.1	99.3

(B) Assemblage produced in Pt capsule

	Spinel	Perovskite	Nepheline
SiO_2	-	-	41.3
TiO_2	10.6	56.1	0.7
Al_2O_3	5.1	1.5	36.6
Fe_2O_3	42.3	-	-
FeO	27.9	1.4	0.6
NiO	4.9	<.1	-
MnO	8.8	0.9	0.3
CaO	0.2	38.8	0.5
Na_2O	-	1.3	19.3
Cs_2O	-	-	1.1
Sum	99.8	100.0	100.4

Starting composition: "SYN-D Glass" Col. 3, Table 1.

Experime.tal conditions: 5 kbar, 1200° for 15 mins, then cool to 900°C over 3 hours.

Table 8. Phase assemblages in slow-cooled "SYN-D Glass 2".

(A) Assemblage produced in Fe capsule

	Pvsk	Sp.	Zirc.	Nepheline	
				(a)	(b)
SiO_2	-	-	-	42.2	43.2
TiO_2	56.8	31.3	34.5	0.1	0.7
ZrO_2	0.2	0.2	45.6	-	-
Al_2O_3	0.2	4.8	1.7	36.4	32.6
FeO	1.3	56.0	4.5	0.3	2.3
MnO	0.7	7.4	1.5	-	0.6
CaO	36.4	0.1	10.2	1.2	2.5
SrO	4.2	-	1.2	-	-
Na_2O	0.6	-	0.4	19.3	16.7
Cs_2O	-	-	-	0.4	1.1
Sum	100.4	99.8	99.6	99.9	99.7

(B) Assemblage produced in Pt capsule

	Pvsk	Sp.	Zirc.	Neph.
SiO_2	-	-	-	43.7
TiO_2	57.1	23.2	30.7	0.6
ZrO_2	<.1	<.1	44.2	<.1
Al_2O_3	0.5	1.6	2.4	34.5
Fe_2O_3	-	21.9	-	-
FeO	1.1	43.8	9.1	2.0
MnO	0.9	8.6	2.2	0.4
CaO	36.7	0.2	10.2	2.1
SrO	3.6	-	0.3	-
Na_2O	0.6	-	0.5	16.3
Cs_2O	-	-	-	0.4
Sum	100.5	99.3	99.6	100.0

Experimental conditions: 5 kbar, 1200° for 15 mins, then cool to 900°C over 3 hours.

crystallizing or quench-produced nepheline. Accordingly, the "cleaner" type (a) nepheline is probably an early-crystallizing phase. Cooling experiments in Pt capsules produced an assemblage of perovskite, spinel, rare zirconolite and type (b) nepheline. No glass was identified in either product assemblage. Mass balance considerations for cesium suggest that trace amounts of a Cs-rich phase may also be present.

6. LEACHING BEHAVIOUR OF HEAT-TREATED SYNROC-D

In view of the preceding evidence concerning the readily-crystallized nature of glasses formed during partial melting of SYNROC D, it seemed desirable to investigate the effect of different cooling rates and annealing temperatures on the leachability of SYNROC-D.

The sample chosen for investigation was S-21, which had previously been prepared by LLL and sent to Savannah River for evaluation. Petrographic studies showed that this sample contained interstitial glass along grain boundaries. Wet-way analyses gave 3.39% Na_2O and 9.48% SiO_2, i.e. a molar SiO_2/Na_2O ratio of 3.5. Formation of the glass had evidently been encouraged by this large ratio and possibly by a hot-pressing temperature somewhat higher than intended. The substantial Sr, Ca and Al leach rates seen in S-21 were probably due to selective leaching of these elements from the glass.

Chips of S-21 were wrapped in platinum foil and placed in evacuated silica tubes. Sample A was heated at 900°C for 3 hours; Sample B was heated at 1075°C for 30 minutes and then cooled to 900°C over 3 hours; Sample C was heated at 1160°C for 30 minutes and then cooled to 900°C over 3 hours. After heat treatment,

the samples were leached in deionized water at 95°C and leachates analyzed for Sr and Ca following established procedures at this laboratory. Results are given in Table 9.

It is seen that the heat treatments have made little difference to the leach rates. This result is surprising since experiments show that any interstitial glass should have become fully crystallized by the heat-treatments to which they were subjected, and that Sr and Ca should have partitioned quantitatively into the perovskite phase, thereby causing a decrease in leach rates.

Further experiments will be necessary to clarify the situation. One possibility is that the effective surface areas of devitrified interstitial glass are increased by crystallization under vacuum and that this effect cancels out the expected decrease in leach rate caused by crystallization of perovskite. This interpretation will be tested by performing experiments on samples which are cooled under pressure. The effects of differing cooling rates should also be explored. Investigations should also be made of the structure of devitrified glass regions by electron microscopy.

7. CONCLUSION

The interstitial glass formed by partial melting of SYNROC-D at 1100-1200°C is silica-poor and alumina-rich. These characteristics are maintained when large variations in SiO_2/Na_2O ratios are imposed, provided that the liquids are buffered by the main SYNROC crystalline phases- spinel, nepheline, perovskite and zirconolite. However, the proportion of glass increases as the SiO_2/Na_2O ratio increases. Glasses of this type possess quite low viscosities and experimental studies show that they are readily

Table 9. Leach rates in S-21 SYNROC-D subjected to various heat-treatments. Units are in multiples of 10^{-5} $g/cm^2.day$.

Day	A	B	C	D (pristine sample)
		Strontium		
1-3	3.0	2.0	1.9	1.0
4-6	3.7	2.0	2.3	1.9
7-12	1.9	1.1	1.1	1.4
12-17	1.9	1.9	2.0	
18-22	4.5	2.2	1.9	
		Calcium		
1-3	1.3	1.2	1.0	1.4
4-6	1.4	0.8	1.0	1.1
7-12	0.8	0.4	0.5	1.1
12-17	0.9	0.8	0.9	
18-22	2.0	1.0	0.9	

crystallized by controlled cooling. The principal phases crystallizing are nepheline, perovskite and spinel, as would be expected for liquids in equilibrium with the SYNROC-D phase assemblage. During crystallization, strontium and calcium are strongly partitioned into the perovskite phase.

The unexpectedly high leachabilities of Ca, Sr and Al seen in S-21 were probably due to selective leaching of these elements from the glass. Surprisingly, the leach rates were not substantially decreased by heat-treating the samples in vacuo so as to devitrify the glass phase. This may have been due to an effective increase of surface area during devitrification. It is hoped that further studies of devitrification at different cooling rates under confining pressure will lead to improved leaching characteristics for calcium and strontium.